THE ASTROPHYSICAL JOURNAL, 441:79–95, 1995 March 1

PAIR CASCADES IN EXTRAGALACTIC JETS. I. GAMMA RAYS

R. D. BLANDFORD AND A. LEVINSON
Theoretical Astrophysics 130-33, Caltech, Pasadena, CA 91125
Received 1994 February 11; accepted 1991 September 9

ABSTRACT

A model of the $\sim$0.1–10 GeV γ-ray jets observed by the EGRET instrument on the *Compton Gamma Ray Observatory* is developed. It is shown that the soft X-ray background in an AGN contributes an opacity to pair production and that a γ-ray photosphere or "γ-sphere" can be defined whose radius increases with γ-ray energy E_γ. It is proposed that the observed γ-ray emission is due to inverse *Compton* scattering of the ambient soft X-rays by relativistic pairs accelerated in situ by shock fronts in a relativistic jet. For a wide range of assumed physical conditions, the emission at a given E_γ originates from near the associated γ-spheres; emission from below the γ-sphere initiates a cascade down to the energy where the γ-rays can escape freely. In this model, the slope of the emergent γ-ray spectrum is determined by the scattered, soft X-ray spectrum and the variation of the particle acceleration rate with jet radius. In general it is expected that the variation in the γ-ray flux will be either slower or later at higher energy. It is also shown that the efficiency of conversion of energy from injected high-energy pairs to 0.1–10 GeV γ-rays is typically high so that the models are radiatively efficient. It is argued that the observed γ-ray jets are likely to be particle-dominated, though magnetically confined. The γ-ray spectrum should continue down to an energy $\sim$5 MeV emitted from an *annihilation radius* within which the pair content of the jet is limited by annihilation. This is probably the site of the beamed hard X-ray emission. It is speculated that the relativistic jets associated with radio-loud AGNs are powered electromagnetically by a spinning black hole and that they are collimated by an encircling MHD wind leaving the accretion disk at a slower speed. Powerful FR2 radio sources are formed when the hole spins rapidly and the relativistic core accelerates the MHD sheath; low-power FR1 sources ensue when the opposite occurs. Finally, it is suggested that the key factor which determines whether or not a given active nucleus can form a jet and a radio to γ-ray nonthermal continuum is the central density of mass-losing stars which, when large, precludes the formation of a super-Alfvénic, collimating wind.

Subject headings: acceleration of particles — galaxies: active — galaxies: jets — MHD — radiation mechanisms: nonthermal

1. INTRODUCTION

The majority of high-energy, extragalactic γ-ray sources observed by the EGRET instrument on the *Compton Gamma Ray Observatory* have been identified with flat spectrum core-dominated radio sources (CRSs) several of which are, more specifically classified as blazars (e.g., Hartman et al. 1992; Thompson et al. 1993). This discovery has been interpreted as implying that relativistic jets, whose presence was first inferred at radio wavelengths, are far more powerful γ-ray emitters. It automatically changes our view of the energetics of extragalactic radio sources on both compact and extended scales and suggests new, diagnostic observations at lower energies. It is also greatly constrains models for the origin of jets and impacts the relationship between the different classes of active galactic nuclei (henceforth AGNs). It is the purpose of this paper to examine one specific class of models of γ-ray jets in this context.

In § 2 we recapitulate what is generally believed about the nature of relativistic jets and some of the major uncertainties. In § 3 we discuss the escape of $\sim$0.1–10 GeV γ-rays from AGNs and introduce the notion of a γ-sphere. It is argued in § 4 that the γ-rays that do escape are most probably produced through inverse Compton scattering by relativistic electrons accelerated in situ, and imhomogeneous, pair-cascade models are described. In § 5 we propose some observational tests and go on to draw some speculative inferences concerning the nature, collimation, and origin of relativistic jets in AGNs.

A preliminary account of some of the ideas contained in this paper has appeared in Blandford (1993).

2. RELATIVISTIC JETS

2.1. *Taxonomy of AGNs*

A minority (between $\sim$3% and 10% dependent upon luminosity) of AGNs are designated as *radio-loud*, the remainder being called *radio-quiet* (e.g., Antonucci 1993). The radio sources belonging to the former class, which are identified with either quasars or elliptical galaxies, are generally further divided into compact (i.e., core-dominant) sources (CRSs) and extended (i.e., lobe-dominant) sources. Many of the core-dominant radio sources exhibit rapidly variable, polarized optical continua and are called *blazars*. The powerful, lobe-dominent radio galaxies are designated FR2 sources, whereas their low-power counterparts are known as FR1 sources. FR1 sources have prominent, two-sided *jets*, and most of the radio brightness distribution is centrally concentrated. In FR2 sources, the highest brightness emission comes from *hot spots* located within the lobes near the source extremities, and the jets are frequently either very faint or one-sided. In bright, core-dominated sources, these jets commonly exhibit *superluminal expansion* indicative of relativistic outflow, which now appears to be characteristic of compact jets in low-power FR1 sources as well (e.g., Laing 1992).

Under the *unified model*, core- and lobe-dominant sources are regarded as members of the same classes, distinguished observationally by the orientation of the observer. The simple view is that in radio-loud AGNs, jets are formed initially with ultrarelativistic speed and the ones that are beamed in our direction are classified as core-dominant. In the blazars, higher frequency, polarized, nonthermal radiation from the jet is also beamed and can overwhelm the roughly isotropic and unpolarized continuum from the active nucleus. The jets in the powerful FR2 radio sources propagate with mildly relativistic speed from the galaxy to the hot spots, where they terminate after passing through a strong shock wave. However, in the weaker FR1 sources, the jets are greatly decelerated in the galactic nucleus and leave the galaxy with little more than the escape velocity. There is a second orientation effect in AGNs, namely that of equatorial obscuration. This has been most convincingly demonstrated in the Seyfert galaxies where many type 2 Seyfert galaxies are believed to be type 1 Seyfert galaxies viewed through an obscuring, equatorial disk (Lawrence & Elvis 1982). Many radio galaxies may likewise be obscured quasars (e.g., Barthel 1993). There is no widely accepted explanation for the difference between radio-quiet and radio-loud objects, although the association of the former with spiral galaxies and the latter with ellipticals is believed to be important.

2.2. γ-Ray Jets

To date, about 40 CRSs (and no extended radio sources or radio-quiet AGNs) have been reported as *EGRET*, 0.1–10 GeV γ-ray sources (Fichtel et al. 1994). Their distances and γ-ray luminosities span a wide range, with the most powerful sources (e.g., 0528+134, 4C 38.41) exhibiting luminosities as high as $10^{49} f$ ergs s^{-1}, (in this paper we adopt $H_0 = 75$ km s^{-1} Mpc^{-1}, $\Omega_0 = 1$), where f is a beaming factor. The apparent exclusive association of *EGRET* AGN sources with compact radio sources strongly suggests that the γ-rays are beamed in a similar fashion to the radio emission so that $f \sim 10^{-3}$ to 10^{-2} and the γ-ray power need not be large compared with the bolometric luminosity. The energy spectra in the range 0.1–10 GeV can be fitted by power laws, with energy spectral indices α_γ in the range 0.7–1.4 (though the broad energy response of the instrument coupled with the paucity of photons cannot really exclude spectral curvature). Some of the *EGRET* AGN sources exhibit rapid time variability, typically on scales of days or weeks (Fichtel & Thompson 1994). In the case of 3C 279, a substantial variation in the $\gtrsim 100$ MeV flux was observed during less than a 2 day interval (Kniffen et al. 1993). In addition, the BL Lac object Mrk 421 has been detected using Cerenkov techniques at energy ~ 0.5 TeV (Punch et al. 1992).

3. THE γ-SPHERE

We have argued that the γ-rays emerging from an AGN are beamed along the jet axis. It is clear that they cannot originate from too small a radius; otherwise they would combine with UVX photons to create electron-positron pairs. It is helpful to define a γ-ray photosphere or *γ-sphere*, of radius r_γ, beyond which the pair-production opacity to infinity equals unity. This will naturally vary with the γ-ray energy, E_γ, and the soft photo flux.

Let us introduce a quantity $\tilde{I}_s(r, \mu, E_s)$ which is the soft photon intensity (power per unit energy, per unit area, per steradian at radius r propagating at an angle $\cos^{-1}\mu$ to the outward jet direction) and *rendered dimensionless by measuring in units of* $c/\sigma_T r$. (The reason for this scaling will become apparent.) For a γ-ray of energy $E_\gamma \gg 1$ (henceforth we measure all energies implicitly in units of $m_e c^2 = 0.51$ MeV unless units are specified directly), the opacity κ_p to pair production is given implicitly by

$$\tilde{\kappa}_p(E_\gamma, r) \equiv r\kappa_p = 2\pi \int_{-1}^{1} d\mu(1-\mu) \int_{\ln[2/(1-\mu)E_\gamma]} d\ln E_s \tilde{I}_s(r, \mu, E_s)\sigma_p(E_s, E_\gamma, \mu)\,, \tag{3.1}$$

where $\tilde{\kappa}_p$ is the *dimensionless opacity*, σ_p (measured like all cross sections henceforth in units of σ_T) is the pair production cross section, which is given by

$$\sigma_p = \frac{3}{16}(1-\beta^2)\left[(3-\beta^4)\ln\left(\frac{1+\beta}{1-\beta}\right) - 2\beta(2-\beta^2)\right], \tag{3.2}$$

and β is the speed of the electron and the positron in the center of momentum frame (e.g., Gould & Schréder 1967). This is related to E_γ and E_s through

$$(1-\beta^2) = \frac{2}{(1-\mu)E_s E_\gamma}\,; \qquad 0 \le \beta < 1\,; \tag{3.3}$$

$\beta = 0, \mu = -1$ corresponds to the threshold for pair production. For a ~ 1 GeV γ-ray the soft photon threshold energy is ~ 0.3 keV. We assume that the spectrum of soft photons is steep enough (specifically that the spectral index $\alpha > -1$) that the opacity is dominated by soft photons just above the threshold energy. The radius of the γ-sphere, $r_\gamma(E_\gamma)$ is then defined implicitly by the equation

$$\int_{\ln r_\gamma}^{\infty} d\ln r\tilde{\kappa}_p = 1\,. \tag{3.4}$$

Equivalently we can invert this equation to introduce an *escape energy* at a given radius r defined by $r_\gamma[E_{\rm esc}(r)] = r$. Only γ-rays with $E_\gamma \lesssim E_{\rm esc}$ can escape.

In order to illustrate the idea of a γ-spheric radius, we consider three simple models of the soft radiation.

3.1. Locally Isotropic, Scattered Nuclear Radiation

We assume that free electrons surrounding the jet within an octave of radius of the γ-sphere (i.e., $r_\gamma - 2r_\gamma$) scatter a small fraction $\langle\tau_T\rangle(r) \propto r^{-q}$ of the soft nuclear spectral luminosity, L_s^n, so that it is roughly isotropic (cf. Begelman & Sikora 1987). Radiation

scattered at both smaller and larger radii is assumed to be unimportant. As we shall see, EGRET γ-spheres for the more powerful sources are typically located within the broad emission line region. The standard emission line clouds are generally modeled to have free electron column densities of $\sim 10^{21}$ cm^{-2} and covering factors ~ 0.1, giving $\langle \tau_T \rangle \sim 10^{-4}$. However, the intercloud medium, which is often invoked as an agent to confine these clouds, is widely supposed to have an electron depth a factor ~ 100 larger (e.g., Netzer 1992). Furthermore, bound electrons, which may have a much greater density than free electrons, will present a roughly Thomson scattering cross section to hard X-rays.

Adopting these simplifications, we can then approximate the isotropic part of the dimensionless intensity by

$$\tilde{I}(r, \mu, E_s) = \frac{k_\tau \sigma_T L_s^n \langle \tau_T \rangle}{8\pi^2 rc}, \qquad \propto r^{-(q+1)}. \tag{3.5}$$

In this equation, k_τ is a model-dependent constant which we calculate to be ~ 1 for $q \sim 0$. Henceforth, we absorb this factor into the definition of $\langle \tau_T \rangle$. For a simple power-law X-ray spectrum, we can write

$$\tilde{I}_s(r, \mu, E_s) = \tilde{I}_s(r, E_\gamma^{-1})(E_s E_\gamma)^{-\alpha} \tag{3.6}$$

If we substitute this intensity into equaton (3.1), and integrate over E_s, μ, r, we obtain

$$\tilde{\kappa}_p = \frac{3\sigma_T}{8\pi rc} L_s^n(E_\gamma^{-1}) \langle \tau_T \rangle A(\alpha), \tag{3.7}$$

where

$$A(\alpha) = \frac{1}{(2+\alpha)} \int_0^1 d\beta\beta \left[(3-\beta^4) \ln\left(\frac{1+\beta}{1-\beta}\right) - 2\beta(2-\beta^2) \right] (1-\beta^2)^\alpha \tag{3.8}$$

and is exhibited in Figure 1. The γ-sphere is located at a radius r_γ that solves the equation $\tilde{\kappa}_p(E_\gamma, r_\gamma) = 1 + q$. Numerically, for $\alpha = 1.5, q = 0$

$$r_\gamma = 0.8 \langle \tau_T \rangle L_{s55}^n [0.26 \text{ keV}] \left(\frac{E_\gamma}{1 \text{ GeV}}\right)^{1/5} \text{pc}, \tag{3.9}$$

where $L_{s55}^n[E_s]$ is the nuclear spectral luminosity in units of 10^{55} s^{-1} at energy E_s.

3.2. *Beamed Radiation*

We next suppose that the soft radiation is beamed in the form of a jet. There are two ways in which this can happen. Either the X-rays are emitted at much smaller radii and are relativistically beamed parallel to the jet or they are created locally in the jet at the radius of γ-ray emission, perhaps by inverse Compton scattering of lower frequency synchrotron radiation photons—the "synchrotron self-Compton process" (e.g., Königl 1981; Maraschi, Ghisellini, & Celotti 1992; Bloom & Marscher 1993).

We approximate the jet as a cone with constant opening semiangle $\theta \ll 1$ and suppose, for simplicity, that the soft radiation, coextensive with the jet, is similarly beamed. (We ignore soft radiation outside the jet.) We also assume that the spectrum is constant with radius, an ssumption which can easily be relaxed, given a more specific model. In this case, the scaled intensity can be written

$$\tilde{I}_s \simeq \frac{\sigma_T}{\pi^2 \theta^4 rc} L_s^j\left(\frac{4}{\theta^2 E_\gamma}, r\right)\left(\frac{E_s E_\gamma \theta^2}{4}\right)^{-\alpha}, \qquad 0 \le 1 - \mu \le \theta^2/2, \tag{3.10}$$

where $L_s^j(E_s, r) \propto r^{-q}$ is the spectral luminosity of the beamed X-rays coextensive with the jet at radius r. Again, performing the integrals, we obtain

$$\tilde{\kappa}_p^j = \frac{3\sigma_T}{16\pi rc} L_s^j\left(\frac{4}{\theta^2 E_\gamma}, r\right) A(\alpha). \tag{3.11}$$

Equation (3.4) gives the γ-spheric radius, r_γ. Aside from the different numerical coefficient and the presence of the optical depth $\langle \tau_T \rangle$, equation (3.11) is similar in form to equation (3.7) for the isotropic case. However, the jet spectral luminosity must be evaluated at a much greater soft photon energy (typically ~ 100 keV for a ~ 1 GeV γ-ray) than is the case for the isotropic emission case (typically ~ 0.3 keV). We shall argue below that in a typical blazar spectrum, the hard ($\gtrsim 1$ keV) X-rays are mostly beamed, whereas the soft ($\lesssim 1$ keV) X-rays are not, and therefore the full hard X-ray flux can be used to estimate L_s^j. In fact, given both radiation components, we can combine equations (3.7) and (3.11) to obtain

$$\frac{\tilde{\kappa}_p^j}{\tilde{\kappa}_p^n} = \frac{1}{2} \frac{L_s^j(4/\theta^2 E_\gamma)}{L_s^n(1/E_\gamma)\langle \tau_T \rangle}. \tag{3.12}$$

Assuming that $\theta \sim 0.1$ and adopting measured soft and hard X-ray fluxes, we find that the opacity due to the beamed hard X-rays dominates that due to the unbeamed soft X-rays as long as $\langle \tau_T \rangle \lesssim 10^{-3}$. We expect that this condition will usually be satisfied.

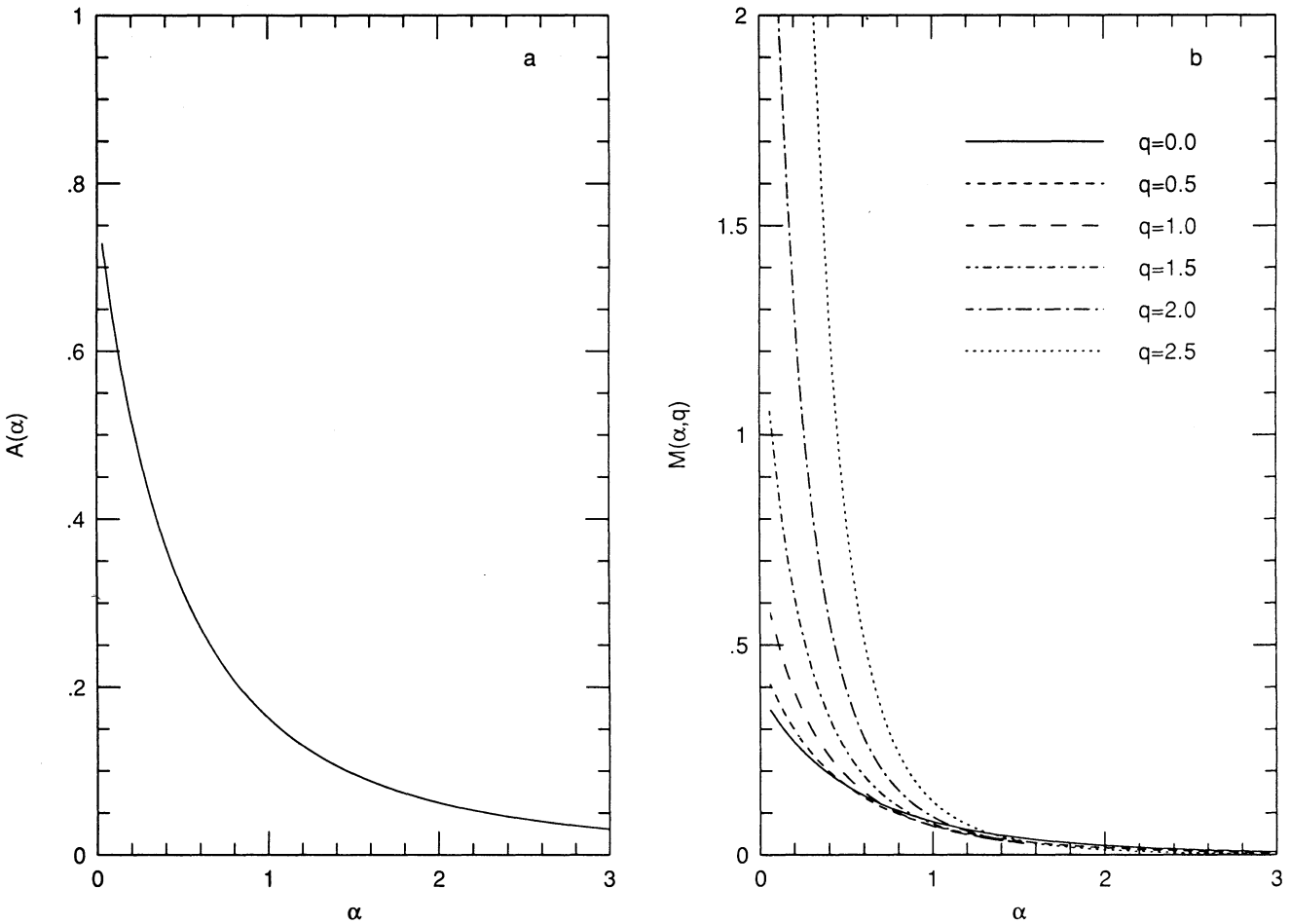

FIG. 1.—(*a*) $A(\alpha)$ and (*b*) $M(\alpha, q)$ vs α. (see text)

3.3. *Radiation Scattered from an Equatorial Disk*

For our third model we suppose that there is a roughly isotropic, power-law, nuclear source of soft photons that is scattered by free electrons in a warped or thick disk so that the spectrum is preserved. This is similar to the models of Begelman & Sikora (1987), Melia & Königl (1989), and Dermer & Schlickheiser (1993, 1994), although we are here concerned with larger disk radii than in these models, and we ignore the radiation that is liberated locally by the gas that accretes inward through the disk. For simplicity, we also suppose that the spectral power scattered per unit log disk radius has a power-law variation and a constant spectral index

$$\frac{dL_s^d}{d\ln R}(E_s, R) \propto E_s^{-\alpha} R^{-q}, \tag{3.13}$$

where R is the disk radius. The dimensionless intensity is then

$$\tilde{I}_s(r, \mu, E) = \frac{\sigma_T}{4\pi^2 rc} \frac{\mu^2}{1-\mu^2} \frac{dL_s^d}{d\ln R} [E_\gamma^{-1}, (\mu^2 - 1)^{1/2} r](E_s E_\gamma)^{-\alpha}. \tag{3.14}$$

Evaluating the pair production opacity, we obtain

$$\tilde{\kappa}_p = \frac{3\sigma_T}{4\pi rc} \frac{dL_s^d}{d\ln R} [E_\gamma^{-1}, (\mu^2 - 1)^{1/2} r] A(\alpha) M(\alpha, q) \tag{3.15}$$

where

$$M(\alpha, q) = \frac{2+\alpha}{2^\alpha} \int_0^1 d\mu (1-\mu)^{1+\alpha} \left[\frac{\mu^2}{(1-\mu^2)}\right]^{1+q/2}. \tag{3.16}$$

$M(\alpha, q)$ is also displayed in Figure 1.

From the form of equation (3.15), we see that the opacity has a similar functional form to that given by equation (3.7) for the isotropic radiation case, as long as we assume that the dominant scattered radiation at jet radius r originates from disk radius $R \sim r$.

For illustration, if we set $\alpha = 1.5$, $q = 0$, we obtain

$$r_\gamma = 0.1 \frac{dL^d_{x55}}{d\ln R}\,[0.26\ \mathrm{keV}, r_\gamma]\left(\frac{E_\gamma}{1\ \mathrm{GeV}}\right)^{1.5}\ \mathrm{pc} \tag{3.17}$$

for the radius of the γ-sphere. Comparing equations (3.9) and (3.17), we find that a disk that scatters a certain fraction of the central radiation from each octave of disk radius is essentially equivalent to a circum-jet medium with an electron scattering optical depth of magnitude ~ 0.1 of this fraction. Without much loss of generality, we therefore concentrate on the isotropic scattering model, adopting $\langle \tau_T \rangle = 0.01$ for illustration purposes.

3.4. *Standard Soft Radiation Spectrum*

Single power laws do not necessarily represent the ambient soft radiation field within an AGN. We are mostly concerned with the isotropic, UV-soft X-ray region of the electromagnetic spectrum which appears to have a steep spectrum $\alpha \sim 1.5$ and is associated with the high-energy extension of the "blue bump" (Laor 1990). We have argued that the beamed radiation from the jet is probably unimportant for determining the location of the γ-sphere. However, other types of AGNs exhibit a flat spectrum $0.5 \lesssim \alpha \lesssim 1$ above ~ 1 keV that is probably isotropic and is overwhelmed by the beamed component in the blazars. In order to estimate the opacity for γ-rays in the $\sim$1–100 MeV energy range, we therefore add a second, isotropic component to our standard radiation spectrum with $\alpha = 0.5$. This probably has a cutoff at around 100 keV (Lin et al. 1993). Our standard soft radiation spectrum has the form

$$\tilde{I}_s = K\left(\frac{E_s}{10^{-3}}\right)^{-0.5}\left[1 + \left(\frac{E_s}{10^{-3}}\right)^{-1}\right]\left(\frac{r}{r_0}\right)^{-(1+q)}, \tag{3.18}$$

where r_0 is an initial radius and for the calculations below, we set $K = 10$. Radiation outside this energy range has relatively little influence, and our results below are surprisingly insensitive to the spectral details.

3.5. *Application to 3C 279, 3C 273, and Mrk 421*

We can illustrate these ideas using three prototypical EGRET sources.

1. The high-polarization quasar 3C 279 (Hartman et al. 1992), has a redshift $z = 0.54$. We suppose that the pair production opacity is dominated by Thomson-scattered soft photons and interpolate between the UV and X-ray observations. We suppose that the soft X-ray emission is nuclear in origin and isotropic. We find that at an observed soft X-ray energy of 0.17 keV, corresponding to an *observed* γ-ray energy of $E_\gamma = 1$ GeV, the associated soft X-ray power (measured in the AGN frame) is of the order $L^n_s \simeq 2 \times 10^{55}\ \mathrm{s}^{-1}$ (Wilkes & Elvis 1987), and we adopt a spectral index $\alpha = 1.5$. (Laor et al. 1994 have found an average X-ray slope of 1.5 in the *ROSAT* band for a sample of PG quasar.) If we assume that $q = 0$, then

$$r_\gamma(E_\gamma) \sim 2\langle \tau_T \rangle \left(\frac{E_\gamma}{1\ \mathrm{GeV}}\right)^{1.5}\ \mathrm{pc}\ . \tag{3.19}$$

In earlier estimates, Blandford (1993) adopted $k_\tau = 2$, $\langle \tau_T \rangle = 10^{-2}$, $q = 0.5$, $\alpha = 0.7$, and $L^n_{x55}(0.6\ \mathrm{keV}) \simeq 5$ to obtain $r_\gamma(1\ \mathrm{GeV}) \simeq 0.1$ pc. Alternatively, Dermer & Schlickeiser (1993) used $k_\tau = 0.5$ and $L^n_{x55}(0.26\ \mathrm{keV}) = 0.7$ to obtain $r_\gamma(1\ \mathrm{GeV}) \simeq 0.006$ pc. Unfortunately, the soft X-ray spectrum and the Thomson opacity are too poorly understood for us to be able to refine this estimate at present. Note that for $\langle \tau_T \rangle \sim 10^{-2}$, $r_\gamma \sim 0.0006$–0.6 pc at EGRET energies. Gamma-ray photospheres are much larger than the putative central black hole, are coextensive with the broad emission line clouds, and are much smaller than the compact radio core.

2. In the case of the $z = 0.16$ quasar 3C 273, we use the source spectrum computed by McHardy et al. (1994, in preparation), with $L^n_s[0.22\ \mathrm{keV}] = 1.1 \times 10^{55}\ \mathrm{s}^{-1}$, $\alpha = 1.75$, and adopt $q = 0$ to estimate that

$$r_\gamma(E_\gamma) \approx 0.7\langle \tau_T \rangle \left(\frac{E_\gamma}{1\ \mathrm{GeV}}\right)^{1.75}\ \mathrm{pc}\ . \tag{3.20}$$

For $\langle \tau_T \rangle \sim 10^{-2}$, $r_\gamma(1\ \mathrm{GeV}) \sim 0.007$ pc. For γ-ray energies $\lesssim 0.5$ GeV, the associated soft photons have observed energy ~ 0.6 keV. Now, the observed X-ray spectrum contains a second component that dominates above ~ 0.6 keV with $\alpha \sim 0.4$ which is probably beamed. We suspect that this hides an isotropic component and that equation (3.20) is an underestimate for $E_\gamma \lesssim 0.5$ GeV.

3. The BL Lac object Mrk 421 has a redshift $z = 0.03$ and a variable X-ray spectrum with an average spectral power $L_s \sim 6 \times 10^{53}\ \mathrm{s}^{-1}$ at $E_s = 0.26$ keV and $\alpha \sim 1$ (George, Warwick, & Bromage 1988). If we suppose that the isotropic component of the soft X-rays has a flux equal to a fraction $f_{\mathrm{iso}} \leq 1$ of the average observed flux, which may be beamed, then

$$r_\gamma(E_\gamma) \sim 0.08 f_{\mathrm{iso}} \langle \tau_T \rangle \left(\frac{E_\gamma}{1\ \mathrm{GeV}}\right)\mathrm{pc}\ . \tag{3.21}$$

Mrk 421 has also been reported as a ~ 0.5 TeV source (Punch et al. 1992). The associated soft photons would lie in the infrared region of the spectrum, and the photospheric radius will be located at $\simeq 11 f_{\mathrm{iso}} \langle \tau_T \rangle$ pc. However, for $E_\gamma \sim 1$ GeV and $\langle \tau_T \rangle f_{\mathrm{iso}} \ll 1$, the γ-sphere can be as small as the black hole. The γ-sphere is necessarily not so well defined and more dependent upon the details of the flow close to the black hole for low-power BL Lac objects and at low γ-ray energies.

4. GAMMA-RAY EMISSION

In the previous section, we showed that there is a minimum, although model-dependent, radius from which γ-rays can escape. How, then, are they emitted? It is possible to argue against a synchrotron origin because the cooling time of an electron emitting ~ 10 GeV γ-rays in a typical magnetic field of strength ~ 1 G is only a few seconds. In order to accelerate electrons to the requisite $\sim$ PeV energies in the presence of such a strong radiation reaction force requires an accelerating field $\gtrsim 1$ MV cm^{-1}, which will exert stresses far higher than those associated with the magnetostatic field. It is also possible to argue against an origin associated with hadronic interactions as there is no evidence for spectral curvature associated with pion decay. Note, however, that these objections do not apply to a proton-initiated synchrotron cascade (Mannheim 1993).

In our view, inverse Compton scattering is the most likely source of the γ-ray emission. The soft photons which are responsible for the γ-ray opacity can also be inverse Compton scattered by relativistic electrons and positrons in order to create more γ-rays. Several models, involving inverse Compton scattering of soft photons by pairs accelerated locally in the jet, have already been proposed. SSC models (e.g., Rees 1967; Königl 1981; Ghisellini & Maraschi 1989), in which a single population of relativistic electrons emits synchrotron radiation at low frequency and inverse Compton scatters the synchrotron photons to much higher frequencies have long been considered. Originally, this was thought of as a two-stage process in which radio photons are first scattered to UV energies, and these UV photons are then scattered as γ-rays (e.g., Bloom & Marscher 1993). Three problems with SSC models can be identified: the γ-ray flux greatly exceeds the naive estimate $\sim F_{\rm UV}^2/F_{\rm rad}$, the γ-ray spectral index differs from the radio and UV spectral indices, and the γ-ray emission appears to be far more variable than the radio emission. This last problem motivates two variants in which the synchrotron spectrum extends into the UV and is once Compton scattered to form the γ-ray spectrum, and, in the second, the synchrotron soft photon source is replaced by a roughly isotropic distribution of scattered soft photons (cf. § 3.1). It is this second variation that we emphasize here.

The original inverse Compton scattering models invoked a single homogeneous source region. Two generalizations are strongly motivated by the EGRET observations. The first is that the scattering electrons form a relativistic jet; equivalently they have an isotropic distribution in a frame moving radially outward with a Lorentz factor Γ. The second generalization is that the source model is inhomogeneous and extends over several octave of jet radius (cf. Königl 1981). We adopt both of these generalizations.

Melia & Königl (1989) and Coppi, Kartje, & Königl (1993) have proposed a model whereby a cold beam of protons with initial energies ~ 10 PeV Comptonize ambient UVX photons to γ-ray energies. A pair cascade quickly develops, and the end result is somewhat similar to some of our models. Dermer, Schlickeiser & Mastichiadis (1992) invoke Comptonization of soft photons coming from an accretion disk that surrounds the putative black hole and impinge upon the jet from behind. At large radii from the central source, these soft photons will be strongly redshifted, as viewed from a frame comoving with the jet, resulting in a relatively small gamma-ray luminosity. To ameliorate this problem, Dermer & Schlickeiser (1993) suggested that the observed γ-rays are produced at smaller jet radii, from an accretion disk at radii extending outside the γ-sphere (cf. § 3.2). By contrast, Sikora, Begelman, & Rees (1994), like us, proposed Comptonization of rescattered radiation. However, in their model, all of the observed emission is produced at a single jet radius. They postulate that internal shocks move outward through a relativistic jet and suggest that this accounts for the observed variability. The emission is produced well outside the γ-sphere and a pair cascade does not develop.

In our model, the pairs are injected with high energy over many octaves of jet radius. At a given radius, the energy of a freshly emitted γ-ray is degraded, via a pair cascade, into many γ-rays with energy near the threshold energy below which the γ-rays can escape to infinity without being further converted into pairs. This threshold energy increases with radius so that higher energy γ-rays tend to orginate from larger radius.

4.1. *Electron Distribution Function*

In most analyses of relativistic jets, it is helpful to consider the emission in a frame that moves outward with respect to the AGN frame with a relativistic speed, and we shall emphasize this approach. It is generally supposed that the emitting particles are distributed isotropically in the comoving frame with an energy that is conserved on the gyrational timescale. On the expansion timescale, the particles will cool through expansion losses, though there may be a compensatory, bulk acceleration of the flow. In addition, there will be radiative drag due to Compton scattering and a compensatory boost of the plasma as γ-rays create fresh pairs. Finally, as we discuss further below, there may be an alternative momentum carrier to the electrons and positrons (for example, Poynting flux or relativistic ions) that can also contribute a bulk acceleration. It is therefore not possible to describe the bulk dynamics of the jet fluid, and the results are sensitive to the assumed radial variation of the jet width and Lorentz factor, Γ. However, this sensitivity is somewhat illusory, as we demonstrate in the Appendix, where we consider the emission from the AGN frame.

In our calculations, we shall adopt the simplest prescription that the jet width and Lorentz factor are constant with radius.

4.2. *Particle Acceleration*

Pair production cannot be the sole source of high-energy particles, and there must be ongoing particle acceleration occurring within the jet. Unfortunately, the mechanism by which the bulk kinetic energy of the outflow is converted into high-energy particles is poorly understood at present. Shock waves are commonly believed to be one of the principal sources of dissipation in jets. They are also known as efficient accelerators. Superluminal motions observed in many of the core-jet sources are often associated with shock waves propagating down the jet. Shock-in-jet models have also been applied to variability observations in CRSs (cf. Marscher & Gear 1985).

The physics of shock acceleration has been studied extensively in the past two decades (e.g., Jones & Ellison 1991). However, the best studied acceleration sites involve nonrelativistic flows and consist of electron-proton plasmas, and, therefore, models that have been developed to treat particle acceleration in those sites are inapplicable to relativistic jets. Hoshino et al. (1992) have developed

detailed models of perpendicular, relativistic shocks in plasmas composed of pairs plus heavy ions, applicable to the Crab Nebula where efficient acceleration is known to occur. They find that relativistic shocks in pure pair plasmas do not give rise to nonthermal distributions of pairs downstream. However, nonthermal pair acceleration does occur when the preshock plasma contains ions having number density much smaller than the number density of pairs but that carry most the upstream bulk energy and may also occur at quasi-parallel relativistic shocks in symmetric pair plasma. If, contrary to the specific assumption that we made above, the jet is an adiabatic, diverging flow, then the bulk Lorentz factor and the Mach number of the flow will increase so that shocks will be more likely to form. It is possible that a balance develops between this kinematic acceleration in which internal energy is converted into bulk kinetic energy and dissipation at shock fronts so that a constant equilibrium bulk Lorentz factor $\Gamma \sim 10$ is maintained. Pairs may also be accelerated directly by inductive electric fields produced by magnetic reconnection.

Again, we settle for simple prescriptions in which particles are injected at energies up to those of the most energetic γ-rays under consideration. Specifically, we shall concentrate upon two prescriptions. In the first we shall inject particles only at high energy and allow them to cascade down in energy so as to emit observable γ-rays. In the second, we postulate that a power-law distribution function is accelerated.

4.3. *Soft Photon Distribution in the Comoving Frame*

The dimensionless soft photon intensity in the comoving frame, $\tilde{I}'_S$ is related to the intensity in the AGN frame through

$$\tilde{I}'_s(r, \mu', E'_s) = (E'_s/E_s)^3 \tilde{I}_s(r, \mu, E_s) , \tag{4.1}$$

with

$$E_s = E'_s \Gamma(1 + B\mu') , \qquad \mu = \frac{\mu' + B}{1 + B\mu'} .$$

Here quantities with primes denote values in the comoving frame, while those without primes refer to values in the AGN frame. We first consider isotropic distribution of the soft photons in the AGN frame with a power-law spectrum $\tilde{I}_s(E_S) = \tilde{I}_0(r)(E_s)^{-\alpha}$; $E_{\min} < E_S < E_{\max}$. As viewed from a frame comoving with the jet, the soft radiation is beamed along the direction pointing toward the central source, and blueshifted by a factor of order Γ. Specifically, we have

$$\tilde{I}'_s(r, \mu', E'_s) = \frac{\tilde{I}_0(r)(E'_s)^{-\alpha}}{\Gamma^{(\alpha+3)}(1 + B\mu')^{(\alpha+3)}} ; \qquad E_{\min} < \Gamma(1 + B\mu')E'_S < E_{\max} . \tag{4.2}$$

Averaging over angles we obtain

$$\tilde{I}'_s(r, E'_s) = \int \tilde{I}'_s(r, \mu', E'_s) \frac{d\mu'}{2} \simeq \tilde{I}'_0(r)(E'_s)^{-\alpha} ; \qquad \Gamma E_{\min} < E'_s < \Gamma E_{\max} , \tag{4.3}$$

where $\tilde{I}'_0(r) = [2^{\alpha+2}\Gamma^{\alpha+1}\tilde{I}_0(r)]/(\alpha + 2)$. Thus, to a good approximation the spectrum in the comoving frame is also a power law with the same index. (At energies below $\Gamma E_{\min}$ the spectrum changes and the intensity declines rapidly with decreasing energy.) A spectrum consists of superposition of power-law spectra is transformed in a similar manner. In what follows we approximate the intensity by

$$\tilde{I}'_s(r, \mu', E'_s) = 2\tilde{I}'_s(r, E'_S)\delta(1 + \mu') . \tag{4.4}$$

4.4. *Kinetic Equations in the Comoving Frame*

We now turn to compute the emission in the comoving frame. We assume that the pairs are distributed isotropically in the comoving frame, and denote by $N'_e(E'_e, r)$ their number density per unit log energy per unit jet radius. (We do not need to distinguish the electrons from the positrons, designating both with the subscript e.) The γ-ray distribution is anisotropic in the comoving frame, reflecting the anisotropy of the soft radiation, and so we introduce the direction cosine as an additional variable. Let $N'_\gamma(E'_\gamma, \mu', r)d\ln E'_\gamma\, d\mu'\, dr$ represent the number of γ-rays at jet radius r between r and $r + dr$, with energy between $\ln E'_\gamma$ and $\ln E'_\gamma + d\ln E'_\gamma$, that are directed into angle element $d\mu'$ in the direction μ'. The evolution of N'_e and N'_γ in the comoving frame is then governed by the equations

$$\Gamma \frac{dN'_e(E'_e, r)}{d\ln r} = -\tilde{\kappa}'_c(E'_e, r)N'_e(E'_e, r) + \int d\ln E_{ei}\, \tilde{\eta}'_{ce}(E'_{ei}, E'_e, r)N'_e(E_{ei}, r) + \int_{-1}^{1} d\mu'(1 - \mu')$$
$$\times \int d\ln E'_\gamma\, \tilde{\eta}'_{pe}(E'_\gamma, E'_e, \mu', r)N'_\gamma(E'_\gamma, \mu', r) - N'_e(E'_e, r) \int R'(E'_e, E'_{ei})N'_e(E_{ei}, r)d\ln E'_{ei} + \tilde{S}'(E'_e, r) , \tag{4.5}$$

$$(\mu' + 1)\Gamma \frac{dN'_\gamma(E'_\gamma, \mu', r)}{d\ln r} = \int d\ln E'_e\, N'_e(E'_e, r)N'_e(2E'_\gamma - E'_e, r)R'(E'_e, 2E'_\gamma - E'_e) - \tilde{\kappa}'_P(E'_\gamma, \mu')N'_\gamma(E'_\gamma, r) + \int d\ln E'_e\, \tilde{\eta}'_{c\gamma}(E'_\gamma, \mu'; E'_e)N'_e(E'_e) . \tag{4.6}$$

(If there are adiabatic losses due to expansion of the jet, an additional term will be present in eq. [4.5].) Here $S'(E'_e, r)$ is the pair injection rate per unit log energy per unit log jet radius, R' is the pair annihilation rate taken from Coppi & Blandford (1990), $\tilde{\eta}'_{ce}$ and $\tilde{\eta}_{pe}$ are the pair distribution functions due to Compton scattering and pair production, respectively, $\tilde{\eta}'_{c\gamma}$ is the γ-ray production rate

due to Compton scattering, and $\tilde{\kappa}'_c$, $\tilde{\kappa}'_P$ are the corresponding opacities. The opacities and redistribution functions are calculated below. Although we have included pair annihilation, we find it to be negligible. One of the advantages of working in the comoving frame is that we could easily include additional processes (e.g., Coulomb scattering, bremsstrahlung, etc.).

To simplify the computations, we averaged equation (4.6) over μ. The angle-averaged γ-ray distribution, $N'_\gamma(E'_\gamma, r) = \int_{-1}^{1} N'_\gamma(E'_\gamma, \mu', r)d\mu'$, is then evolved according to the equation

$$(\xi + 1)\Gamma \frac{dN'_\gamma(E'_\gamma, r)}{d\ln r} = -\zeta_1 \tilde{\kappa}'_P(E'_\gamma)N'_\gamma + \zeta_2 \int d\ln E'_e \tilde{\eta}'_{c\gamma}(E'_e, E'_\gamma)N'_e(E'_e) + \int d\ln E'_e N'_e(E'_e, r)N'_e(2E'_\gamma - E'_e, r)R'(E'_e, 2E'_\gamma - E'_e)\,, \quad (4.7)$$

where $\xi < 1$, ζ_1, and ζ_2 are parameters of order unity (which depend in general on radius and energy), $\tilde{\kappa}'_P(E'_\gamma) = \int_{-1}^{1} d\mu' \tilde{\kappa}'_P(E'_\gamma, \mu')$, and $\tilde{\eta}'_{c\gamma}(E'_e, E'_\gamma)$ is given by equation (4.16). Similarly, we define $\tilde{\eta}_{Pe}(E'_\gamma, E'_e)$ to be the angle-averaged pair production rate. The accuracy of the computations was checked using the relation

$$\int d\ln E'_\gamma E'_\gamma N'_\gamma(E'_\gamma, r) + \int d\ln E'_e E'_e N'_e(E'_e, r) = \Gamma^{-1} \int^{\ln r} d\ln r' \int d\ln E'_e E'_e \tilde{S}'(E'_e, r')\,. \quad (4.8)$$

4.5. *Pair Production*

In § 3 we presented three models for the distribution of soft photons and computed the resultant opacities. We now calculate the associated energy distribution functions for the created pairs. As we are dealing with hard γ-rays, $E'_\gamma \gg 1$, we can ignore the energies of the soft photons.

If μ_{CM} is the cosine of the angle between the γ-ray momentum and either the electron or the positron momentum in the center of momentum frame, then the electron and positron energies are given by

$$E'_e = \tfrac{1}{2}E'_\gamma(1 \pm \beta_{CM}\mu_{CM})$$

where

$$\beta_{CM} = \left[1 - \frac{2}{(1 - \mu')E'_s E'_\gamma}\right]^{1/2} \quad (4.9)$$

is the pair speed in the center of momentum frame and μ' is the cosine of the angle between the soft photon direction and the γ-ray in the comoving frame. (Note that the sum of the electron and positron energies equals the incident γ-ray energy.)

We can now define the pair redistribution function, which is the pair production rate per unit log energy E'_e and per unit log radius r,

$$\tilde{\eta}'_{pe}(E'_\gamma, \mu', E'_e) = 2\pi \int_{\ln[2/(1-\mu')E_\gamma']} d\ln E'_s \tilde{I}'_s(r, E'_s) \frac{d\sigma'_p}{d\ln E'_e}(E'_s, E'_e, \mu') \quad (4.10)$$

where

$$\frac{d\sigma'_p}{d\ln E'_e} = \frac{2E'_e}{\beta_{CM}E'_\gamma}\frac{d\sigma'_p}{d\mu_{CM}} = \frac{3}{8}\frac{(1 - \beta_{CM}^2)E'_e}{E'_\gamma}\left[\frac{1 + \beta_{CM}^2(2 - \mu_{CM}^2)}{1 - \beta_{CM}^2\mu_{CM}^2} - \frac{2\beta_{CM}^4(1 - \mu_{CM}^2)^2}{(1 - \beta_{CM}^2\mu_{CM}^2)^2}\right]. \quad (4.11)$$

Here $d\sigma'_p/d\ln E'_e$ is the differential cross section in units of the Thomson cross section. This expression includes both electrons and positrons and is valid for $0 \le E'_e \le E'_\gamma$ under our approximation. Look up tables for $\tilde{\eta}'_{pe}(E'_\gamma, \mu', E'_e)$ were computed numerically for the soft photon spectra considered above. The soft photon opacity is then given by

$$\tilde{\kappa}(E'_\gamma, \mu') = \tfrac{1}{2}\int^{\ln E_\gamma'} d\ln E'_e \tilde{\eta}'_{pe}(E'_\gamma, \mu', E'_e)\,. \quad (4.12)$$

4.6. *Compton Scattering*

In the rest frame of the electron the Compton scattering kernel is given by

$$\sigma_C^{ER}(E_{\gamma i}^{ER} \to E_{\gamma f}^{ER};\ \mu_i^{ER} \to \mu_f^{ER}) = dN^{ER}\sigma_{KN}\,\delta(\xi^{ER} - 1 + 1/E_{\gamma i}^{ER} + 1/E_{\gamma f}^{ER})\,, \quad (4.13)$$

whre dN_e^{ER} is the number density of rest frame electrons, ξ^{ER} is the cosine of the angle between the incident and scattered photons, and σ_{KN} is the Klein-Nishina cross section (in units of σ_T) in the electron rest frame. Here the superscript ER refers to quantities measured in the electron rest frame. Transforming to a frame that moves at velocity β' with respect to the rest frame we have

$$\sigma'_C = \frac{D'}{D'_1}\sigma_C^{ER}\,; \qquad E_{\gamma i}^{ER} = D'E'_e E'_{\gamma i}\,; \qquad E_{\gamma f}^{ER} = D'_1 E'_e E'_{\gamma f}\,, \qquad 1 - \xi^{ER} = \frac{1 - \xi'}{E_e'^2 D' D'_1}\,; \qquad dN_e^{ER} = \frac{dN'_e}{E'_e}\,,$$

with $D' = (1 - \beta'\mu'_i)$, $D'_1 = (1 - \beta'\eta)$ where $\cos^{-1}\eta$ is the angle between the emitted photon and β'. Combining all these results we obtain

$$\sigma'_C(E'_{\gamma i} \to E_{\gamma f};\ \xi') = \frac{3\,dN'_e}{16\pi E'_e E_{\gamma i}'^2}\left[1 + \left(1 - \frac{1 - \xi'}{E_e'^2 D' D'_1}\right)^2 + \frac{E'_{\gamma i}E'_{\gamma f}(1 - \xi')^2}{E_e'^2 D' D'_1}\right]\delta[\xi' - 1 + (E'_e D'/E'_{\gamma f} - E'_e D'_1/E'_{\gamma i})\,. \quad (4.14)$$

The rate of γ-ray production per unit log E_γ per unit log r, due to Compton scattering of soft photons with intensity $\tilde{I}$ by a beam of electrons of density dN'_e and velocity β is then given by

$$d\tilde{J}'(E'_\gamma, \mu', \beta') = E_\gamma \int \sigma'_C(E'_S \to E'_\gamma; \mu')\tilde{I}_S(E'_S)d\ln E'_S \, .$$

To obtain the emission function due to an isotropic distribution of electrons we must average over the angles between the directions of the electron and the incident photon. The result is lengthy. However, the energy of the scattered photon is significantly larger than the soft photon energy, and to a good approximation we can neglect the latter. To lowest order in E'_S/E'_γ, the Compton redistribution function can be written in the form

$$\tilde{\eta}'_{c\gamma}(E'_\gamma, \mu'; E'_e) \equiv \frac{d\tilde{J}'}{dN'_e} = \frac{E'_\gamma}{4\beta' E'_e(E'_e - E'_\gamma)} \int_{\ln\{[(1-\beta')E_e'E_\gamma']/[(1-\beta'\mu')E_e' - (1-\mu')E_\gamma']\}}^{\ln E_{\max}'} E_S'^{-1}\tilde{I}'_S(E'_S)d\ln E'_S \, . \tag{4.15}$$

The opacity to Compton scattering and the angle-averaged Compton redistribution functions are then defined through

$$\tilde{\kappa}'_c(E'_e) = \int_{E_\gamma' < E_e'} d\ln E'_\gamma \int_{-1}^{1} \tilde{\eta}'_{c\gamma}(E'_\gamma, \mu'; E'_e)d\mu' \, , \tag{4.16}$$

$$\tilde{\eta}'_{c\gamma}(E'_e, E'_\gamma) = \int_{-1}^{1} \tilde{\eta}'_{c\gamma}(E'_\gamma, \mu'; E'_e)d\mu' \, , \tag{4.17}$$

$$\tilde{\eta}'_{ce}(E'_{ei}, E'_{ef}) = \frac{E_{ei}}{E_{ei} - E_{ef}} \int_{-1}^{1} \tilde{\eta}'_{c\gamma}(E'_{ei} - E'_{ef}, \mu'; E_{ei})d\mu' \, . \tag{4.18}$$

For the soft photon intensity given by equation (3.18), the above integrals can be easily performed analytically.

4.7. *Numerical Scheme*

Equations (4.5) and (4.7) were differenced and integrated numerically starting from a fiducial radius $r = 1$ for energies encompassing the EGRET energy range, $200 \lesssim E_\gamma, E_e \lesssim 2 \times 10^4$. On transforming to the comoving frame, the γ-ray energy is redshifted by a factor $\sim\Gamma$. An energy bin width $\Delta\ln(E) \sim 0.025$ was found to be adequate and Compton scatterings of low-energy photons that left the recoiling electron in the same energy bin turned out to be ignorable. As expected, the dominant source of γ-rays in the EGRET energy interval turned out to be Compton scattering by electrons with energy $\gtrsim 2E_\gamma$ of soft photons with energy $E_s \lesssim E_\gamma^{-1}$ from near the relevant γ-sphere. In addition to the explicit particle acceleration source term, the dominant sources of pairs were secondary production by γ-rays of energy $\sim 2E_e$ combining, at threshold, with soft photons of energy $\sim E_e^{-1}$. Sample pair production and Compton redistribution functions are presented in Figure 2.

4.8. *Numerical Results*

For our standard source model we choose a locally isotropic soft photon distribution function in the AGN frame with $\tilde{I}_s$ given by equation (3.18). In the examples presented below, the boundary conditions chosen at $r = r_0 = 1$ are $N_\gamma = N_e = 0$. In general we find that the asymptotic spectra are highly insensitive to boundary conditions, provided that r_0 is small enough.

We find that if pair acceleration is sufficiently efficient [specifically, if the injected spectrum is flatter than about $\tilde{S}'(E'_e) \propto (E')^{-1.5}$], then the pair cascade spectra well within the γ-ray ray jet are power laws with indices ~ 1.7–1.8 (but are slightly curved at high energies for delta function injection), and are highly insensitive to the spectra of injected pairs and soft photons. This is partly due to the fact that for our standard spectrum ($\alpha > 1$ at energies below ~ 0.5 keV) the injected pairs are cooled predominantly by "blue bump" photons (see § 5), and partly due to the fact that the pair cascade process smooths out features associated with the soft radiation spectrum. The dominant imprint of the soft spectrum is a slight curvature of the emergent γ-ray spectra (cf. Fig. 4) which is mostly due to the sharp cutoff of the soft spectrum at ~ 100 keV.

Figure 3 shows emergent γ-ray energy spectra, $\Phi \equiv E_\gamma N_\gamma(r = \infty)/S_0$, normalized to the total energy injected in the AGN frame, $S_0 = \int \tilde{S}\, dE_e\, d\ln r$, which were computed using $\tilde{S}'(E'_e, r) = S'_0\, r\, \delta(r - r_0)\delta(E'_e - E'_{\max})$ with $E'_{\max} = 5$ GeV (50 GeV in the AGN frame), and $q = 0$. Here Φ is the fraction of the total energy injected as particles that emerges in γ-rays per unit $\ln(E_\gamma)$. The numbers that label the curves are the values of the injection radius, r_0, in units of r_γ(1 GeV). As can be seen, a significant fraction of the energy injected emerged in the form of γ-rays having energies near the threshold energy at which the γ-spheric radius equals the injection radius, reflecting the mapping between γ-ray energy and γ-spheric radius discussed in § 3. The efficiency for γ-ray production in the EGRET range increases with increasing injection radius and approaches 50%–60% for $r_0 \gtrsim r_\gamma$(1 GeV).

Figure 4 shows the development of the γ-ray spectrum down the jet. The γ-ray spectra were all calculated for standard soft spectra with $q = 0$, 1, and $\tilde{S}'(E'_e, r) \propto \delta(E'_{\max} - E'_e)r^{-(1+p)}$; $p = -1$ corresponds to constant injection rate per unit logarithmic radial increment. The development of the spectrum depends upon the radial variations of the pair injection rate and soft photon intensity. In Figures 4*a* and 4*b* the soft photon intensity declines more rapidly with radius than the pair injection rate ($p < q$), and it is seen that the spectrum harden with radius, whereas the reverse holds in Figure 4*c*. Figure 4*d* presents self-similar solution. The soft radiation intensity and the pair source function, in this example, have the same radial dependence, and it is seen that the spectrum converges to its asymptotic form very close to the fiducial radius $r = 1$ and is maintained in its form as the radius increases. The emergent γ-ray spectra are slightly curved, with average γ-ray spectral indices approximately given by $\alpha_\gamma \sim \bar{\alpha}(1 + p)/(1 + q)$, where $\bar{\alpha} \sim 1$ is the average soft X-ray spectral index, which is expected if the asymptotic flux is dominated by γ-rays that emerged from near to their associated γ-spheres.

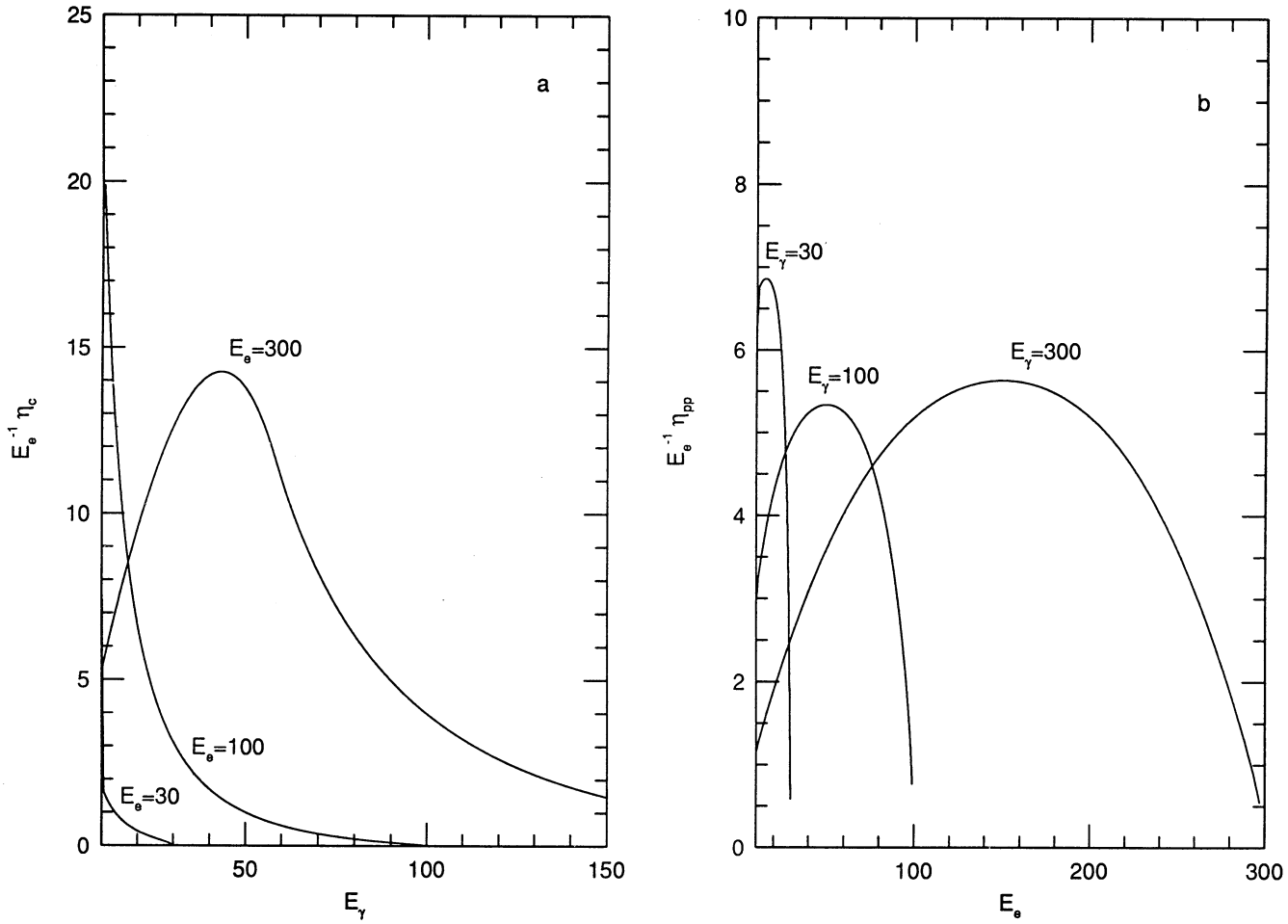

FIG. 2.—Gamma-ray production rate, due to inverse Compton scattering, per unit log E_γ, vs. γ-ray energy for pair energies of 30, 100, and 300 MeV. (*b*) Pair production rate per unit energy for γ-ray energies of 30, 100, and 300 MeV.

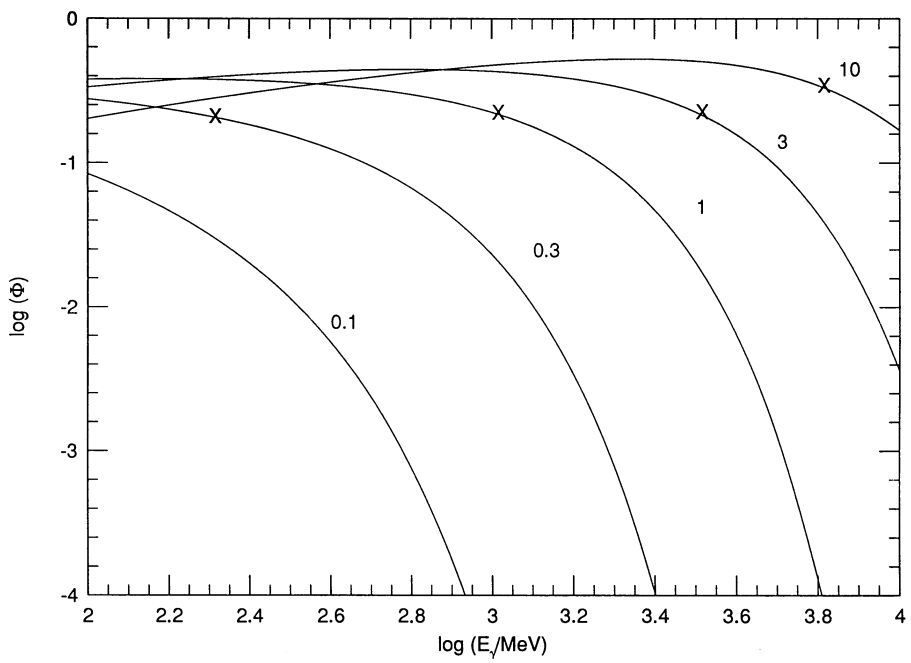

FIG. 3.—Emergent γ-ray spectrum for particle injection at energy $E_\gamma = 5$ GeV in the comoving frame, and bulk Lorentz factor $\Gamma = 10$. The single injection radius in units of the γ-spheric radius at $E_\gamma = 1$ GeV labels the curves. The ordinate is the spectral efficiency $\Phi = E_\gamma N_\gamma / \int \tilde{S}\, dE_e\, d\ln r$ (see § 4.8). The γ-ray energy for which the γ-spheric radius equals the injection radius is denoted with a cross.

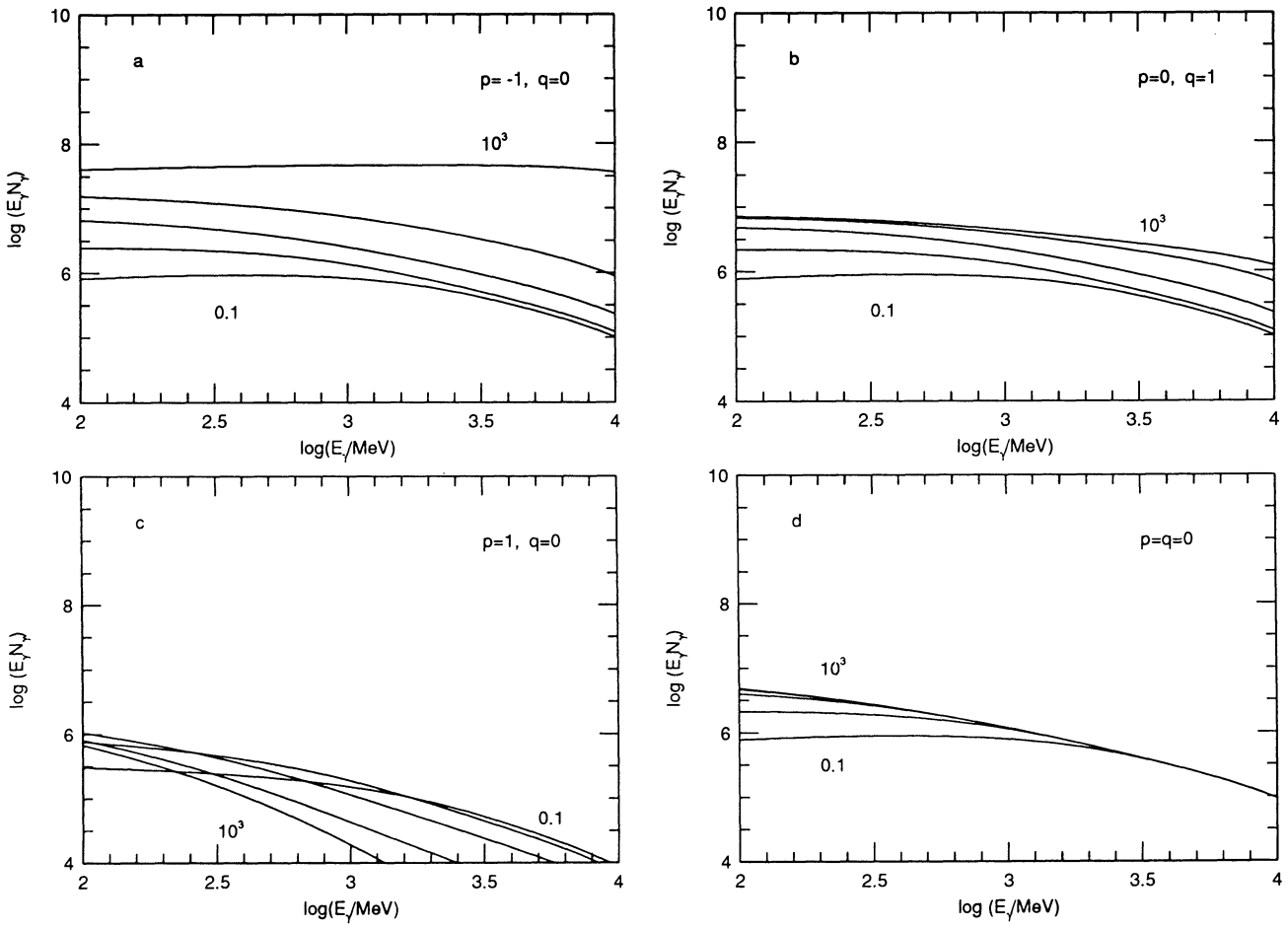

FIG. 4.—Local γ-ray spectra exhibited as spectral efficiencies with arbitrary normalization. The four cases correspond to $q \equiv d \ln \langle \tau \rangle / d \ln r = 0$, 1 and $p \equiv d \ln \tilde{s} / d \ln r = -1, 0, 1$. The curves in the window are labeled by radius relative to r_γ(1 GeV) and show the emergent spectrum development with radius.

The emergent pair spectrum is typically steeper than the γ-ray spectrum, with only a small fraction (a few percent) of the total power injected carried by pairs having energies in excess of the EGRET range.

To examine the sensitivity of the results to changes in the pair injection rate and soft photon intensity, we computed spectra for different soft radiation intensities and particle source functions (Fig. 5.). Figures 5*a* and 5*b* show emergent spectra calculated using the same source function as in Figure 3, but a single power-law soft-photon intensity with $\alpha = 0.5$ (*a*) and 1.5 (*b*). As can be seen, the emergent γ-ray spectrum is slightly softer at high energies in the latter case, reflecting the steepness of the soft radiation spectrum. Typically, we find that the emergent γ-ray spectrum is not very sensitive to changes in the soft radiation intensity. We also find that the overall γ-ray production efficiency in the EGRET range is smaller, and that the emergent spectra are steeper for power-law injection, $\tilde{S} \propto E_e'^{-2}$ (Fig. 5*c*), comparing with delta function injection (in energy). For example, for $p = -1$, $q = 0$, the efficiency in former case is less than 20%, whereas in the latter case it exceeds 60%.

5. GENERAL IMPLICATIONS

In this paper we have outlined one particular interpretation of the surprisingly intense γ-ray fluxes observed by EGRET from many CRS. We have proposed that the γ-rays are ambient soft photons, Compton scattered by relativistic electrons and positrons. We have shown that if the particle acceleration is sufficiently "plutocratic" so that most of the power is injected in particles with energy in excess of the EGRET range, ($E_e \gg 10$ GeV), then a pair cascade will develop and that power-law γ-ray spectra with slopes in roughly the observed range will be produced.

We have considered three distinct sources of soft photons, Thompson scattering of a central continuum source by infalling, ionized gas, an accretion disk, and the jet itself. For each of these sources we can define an energy-dependent γ-ray sphere at a radius $\sim 10^{15}$–10^{18} cm dependent upon the overall AGN luminosity. We have argued that the γ-rays of a given energy are probably created near their γ-spheres, provided that the rate of particle injection declines sufficiently rapidly with radius (specifically if the exponent $p > q$). The slope of the emergent spectrum will reflect the radial dependence of the particle acceleration. Under these conditions, the radiative efficiency with which the power injected in the form of high-energy particles is transformed into γ-rays with energy in the EGRET range can be quite high, typically $\gtrsim 60\%$.

We now turn to the more general implications of this model and its relationship to other manifestations of jets.

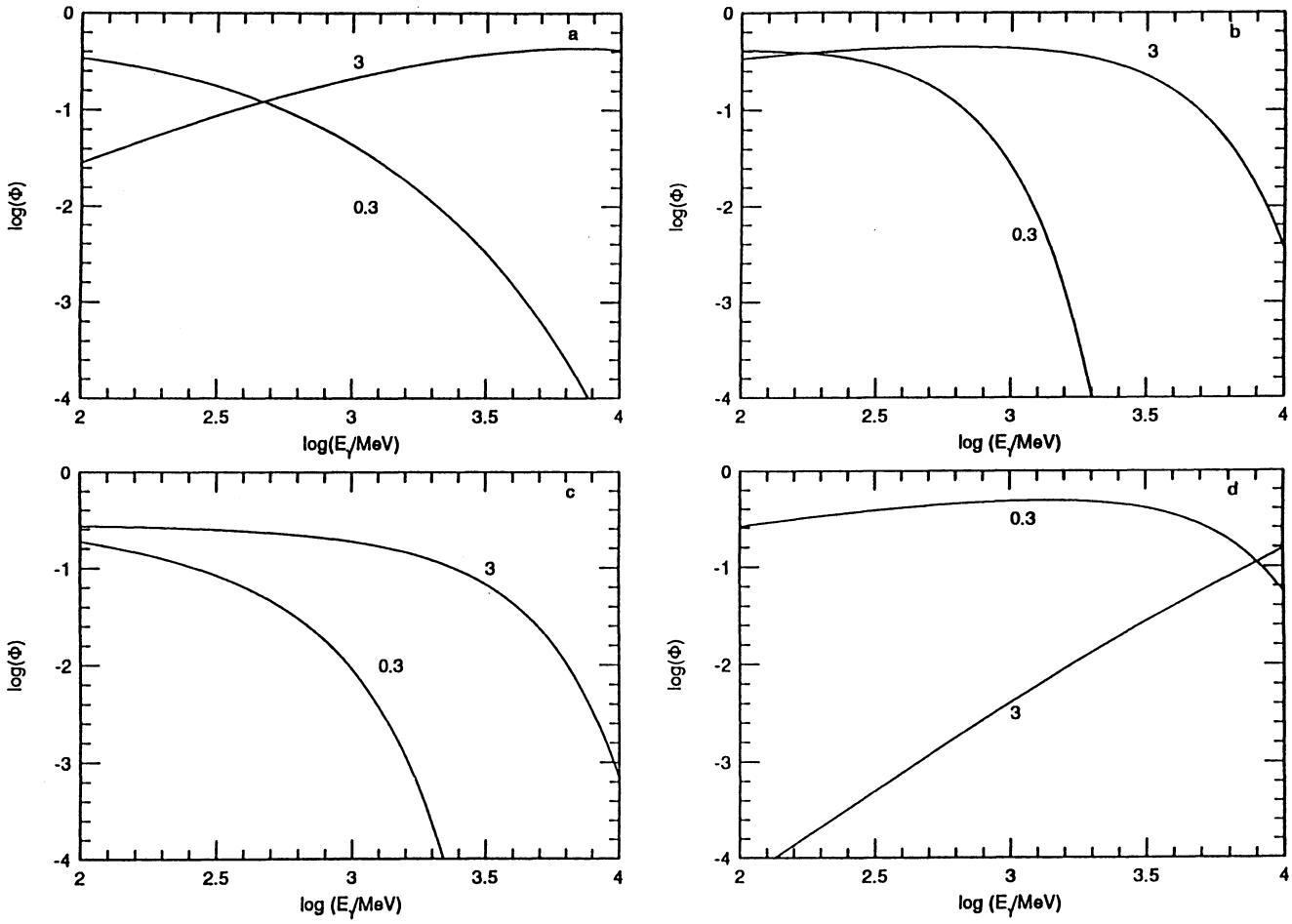

FIG. 5.—Spectral efficiency, Φ, for (*a*) $\hat{I}_s \propto E_s'^{-0.5} r^{-2}$, (*b*) $\hat{I}_s \propto E_s'^{-1.5} r^{-2}$, (*c*) standard soft spectrum with $q = 0$, $\tilde{S} \propto E_e'^{-1}\,\delta(r - r_0)$, and (*d*) standard soft spectrum with $q = 1$. In (*a*), (*b*), and (*d*), $\tilde{S} \propto \delta(E_e' - E_{\max})\delta(r - r_0)$ with $E_{\max}' = 5$ GeV. Curves are labeled by $r_0/r_\gamma(1\ \mathrm{GeV})$.

5.1. *Energetics*

The high radiative efficiency has an important corollary, namely, that relativistic electrons with energy well in excess of the escape energy at a given radius, $E_{\rm esc}(r)$ are able to cool radiatively in a time short compared with the time it takes them to flow through a distance r. Conversely, much less energetic electrons will not lose much of the energy to inverse Compton scattering of EGRET γ-rays. In fact it can be shown that when $\alpha < 1$ the radiative cooling time measured in the AGN frame is given approximately by

$$t_{\rm cool}(E_e, r) \sim \frac{r}{c}\left[\frac{E_{\rm esc}(r)}{E_e}\right]^{\alpha}; \qquad E_e < E_{\rm esc}\ . \tag{5.1}$$

(In our standard model $\alpha > 1$ and the cooling at low electron energy is greater, see below.) It is the similarity of the Compton scattering and pair production cross sections near threshold energies that underlies this relationship and guarantees the high efficiency. In many of the observed EGRET sources the observed γ-ray flux significantly exceeds the flux observed at lower frequencies. This implies that the synchrotron emission must be smaller than the inverse Compton emission, and, consequently, that the magnetic energy density in the comoving frame is generally less than the soft radiation energy density, which in turn, is less than the γ-ray energy density. Therefore, γ-ray jets as described here cannot be dominated by electromagnetic energy flux. (Of course, not all bright CRSs have been detected by EGRET, and it remains possible that the unobserved jets are primarily electromagnetic.)

The local electron distribution functions that we computed generally exhibit an accumulation of particles below the threshold energy where radiative cooling is ineffective. This means that, at a given radius, most of the energy density is carried by the lowest energy particles that have accumulated from smaller radii. Furthermore, most of the momentum flux in the jet should also be carried by the lowest energy electrons. Therefore, γ-ray jets need not be radiatively decelerated and can increase their bulk Lorentz factors as described above. Indeed, as the jet expands, the escape energy increases so that radiative drag becomes decreasingly significant. Even if the jets have only mildly relativistic bulk speeds at small radii, they can still accelerate to give $\Gamma \sim 10$ at larger radii. For example, in the limiting case of an ultrarelativistic, adiabatic jet, with a pressure declining $\propto r^{-2}$, the bulk Lorentz factor can accelerate according to $\Gamma \propto r^{1/2}$ (Blandford & Rees 1974).

Unfortunately, most γ-ray jets have not been detected in the few MeV energy range which probably contributes the majority of their observed γ-ray energy flux. Two exceptions are 3C 273 and 3C 279 (Hermsen et al. 1993) for which the energy flux per octave

appears to be roughly constant or slowly decreasing above a few MeV. The break energy measured in the AGN frame is found to be 1–30 MeV. The total γ-ray power in 3C 279 varies between (2–10) $\times 10^{45}$ ergs s^{-1} if we adopt a beaming angle $\theta = 0.1$. It is clear that jets, at least those observed by EGRET, are not incidental, by-products of nuclear activity, but comprise a major channel for the total power released in accretion of gas onto a spinning black hole.

The approximations that we used to compute the electron scattering and pair production in § 4 are less accurate around $\sim m_e c^2$. Nevertheless, γ-spheres should still be present all the way down to their *annihilation radii*, $r_{\rm ann}$, within which the pair density is limited by annihilation. This means that for $r \ll r_{\rm ann}$ all the pairs can cool on the expansion timescale and annihilate. The radiative efficiency can still be high at the annihilation radius. For the majority of sources for which the EGRET γ-ray spectral indices satisfy $\alpha_\gamma \gtrsim 1$, the fraction of the total jet power that is radiated away will be dictated by the efficiency of particle acceleration near the γ-sphere for the energy where $\alpha_\gamma \sim 1$. Conversely, for the minority of sources for which the EGRET $\alpha_\gamma < 1$, most of the γ-ray flux is emitted at large radius, presumably because the particle acceleration is relatively more efficient there. (It is also possible that the observed γ-ray energy flux is not proportional to the emitted flux because the solid angle within which the emission is beamed changes with radius due to changes in either γ or θ.)

5.2. *Jet Confinement*

Concomitant with estimates of the energy flux are estimates of the minimum pressure within the γ-ray jets. For a relativistic electron-positron jet carrying a power $L_j = 10^{46} L_{j46}$ ergs s^{-1}, and moving with a Lorentz factor Γ, the internal particle pressure $p_3 = 10^3 p_3$ dyne cm^{-2} at radius $r = 10^{16} r_{16}$ cm must satisfy

$$p_3 \gtrsim L_{j46} (\Gamma\theta)^{-2} r_{16}^{-2} , \tag{5.2}$$

where θ is the jet opening angle. (We can assume that $\Gamma\theta \sim 1$ if a cascade develops.) If the jet is confined transversely by an electron-ion plasma for which the rms ion speed (thermal plus bulk motion) is comparable with the escape speed from the central mass as it propagates from radius r to radius $2r$, then it is straightforward to show that the Thomson optical depth associated with this gas over this radius interval will satisfy

$$\tau_{\rm T}(r) \gtrsim \frac{L_j}{L_{\rm Edd}} (\Gamma\theta)^{-2} \tag{5.3}$$

independent of radius, with $L_{\rm Edd}$ being the Eddington luminosity associated with the central mass.

It may be difficult to satisfy this inequality, especially in the case of quasars. For example, with 3C 279 in a quiescent state, we have argued that the ~ 10 GeV γ-sphere is at $r \sim 10 \langle \tau_{\rm T} \rangle$ pc. An upper limit on the central mass, based on the mass determinations in nearby galactic nuclei (e.g., Kormendy 1992), is $M \lesssim 10^9 M_\odot$. This, in turn, implies that $L_{\rm Edd} \lesssim 10^{47}$ ergs s^{-1}, and consequently $\langle \tau_{\rm T} \rangle \gtrsim 0.1$. This largely exceeds the Thomson depth inferred from the absence of very broad, electron scattering wings in the highest ionization emission line profiles, which are believed to originate from radii $\lesssim 10^{18}$ cm (Shields & McKee 1981). Although this argument, which is similar to the argument that has been used on larger length scales, does not completely preclude thermal pressure confinement, it does motivate consideration of magnetic confinement models in which γ-ray jets are pinched by toroidal magnetic field derived from a spinning accretion disk. Now, we have argued above that magnetic fields are dynamically unimportant within observed γ-ray jets. This implies that if they are magnetically confined, then the poloidal current flows along the jet surface. Alternatively, if jets are confined by thermal pressure, then the electron scattering optical depth is likely to be so large that the γ-ray photosphere must be determined by Thomson scattering.

5.3. *Jet Velocity*

There is every expectation that, in a real jet flow, the velocity will vary both transversely and along the jet. In § 4 we outlined a simple model for a constant Lorentz factor jet. The value of this Lorentz factor can only be bounded from the variability time which should not exceed $\sim r/\Gamma^2 c$. For 3C 279, this merely requires that $\Gamma \gtrsim 3$ consistent with the value $\Gamma \sim 10$ suggested by estimates of the beaming factor. There are indications from observations of intraday variability (e.g., Quirrenbach et al. 1991), that larger Lorentz factors, up to $\Gamma \sim 100$, might be present in some radio cores which are found at radii significantly larger than those of the γ-ray jets. However, observations of radio jets on a yet larger scale suggest an overall deceleration to a speed $\sim c/2$ (Bridle & Perley 1984). As we discussed in § 4.2, the bulk Lorentz factor of a relativistic jet can both increase and decrease depending upon the balance between kinematic acceleration and the formation of shock fronts. Furthermore a real jet is likely to be a shear flow which allows an observer to see a range of jet Lorentz factors Γ inclined with respect to the observed direction by angles $\lesssim \Gamma^{-1}$. Fortunately, as we explain in the Appendix, the partition of particle energy between bulk and internal energy is relatively unimportant for the production of γ-rays.

5.4. *Relationship to Radio-X-Ray Observations of CRSs*

CRSs are also observed from low radio frequencies to hard X-ray energies. The radio to optical emission is highly polarized and variable and generally attributed to beamed synchrotron emission from the jet. Many quasars exhibit additional "blue bumps" that are generally unpolarized and are supposed to be thermal emission from gas accreting near to the black hole. The origin of the X-rays is more problematic. Often CRS X-ray spectra are decomposed into a superposition of a steep spectrum component dominating below ~ 1 keV and a flatter component observed at higher energy. In § 3.4 we interpreted the soft X-rays as the high-energy extension of the thermal emission spectrum, deriving from near to the black hole. The hard X-rays, we associate with the jet. (In the case of 3C 273, McHardy et al. 1994 have presented evidence that the hard X-ray component, and not the soft X-ray component, correlates with the millimeter variation, leading it by ~ 10 days which is consistent with this view.)

In § 5.1 we argued that inverse Compton scattering by relativistic pairs may extend down to energies of a few MeV with smaller associated γ-spheres. Lower energy photons (with $E_\gamma \lesssim 0.5$ MeV) are not subject to significant absorption through pair production,

and so for them there is no γ-sphere. Now, as shown in Figure 3, the γ-ray spectrum emitted by the pairs at a given radius is a hard spectrum with a high-energy turnover at $E_{esc}(r)$. We generally assumed that the contribution to the emergent spectrum from a given radius r at an energy $E_\gamma \ll E_{esc}(r)$ is small compared with the contribution from the γ-sphere, $r_\gamma(E_\gamma)$ at smaller radii. However, this will no longer be so below ~ 0.5 MeV, and it is quite reasonable that the hard, power-law beamed X-rays in the energy interval 1 keV $\lesssim E_\gamma \lesssim 0.5$ MeV, which overwhelms the nuclear spectrum in the blazars, is just inverse Compton scattering of the "blue bump" soft photons by relativistic pairs accelerated at the start of the γ-ray jet. The infrared and optical CRS continua are most likely to be synchrotron emission from comparable radii.

The radio emission is also believed to be synchrotron emission but from radii much larger than those associated with the γ-rays. The majority of compact radio sources exhibit flat-spectrum cores, unresolved by VLBI, plus one-sided, steeper spectrum jets (Pearson 1989). The cores are supposed to be the optically thick inner parts of the jets with radio photospheres that decrease in size with increasing frequency (in contrast to those of the γ-spheres). The resolved radio jets are generally presumed to be regions of optically thin synchrotron emission and often contain features that move outward with apparent superluminal speed, indicative of bulk relativistic motion with Lorentz factors $\Gamma \sim 10$. The millimeter and submillimeter photospheres should be smaller than the radio photospheres and may be comparable in size to the $\gtrsim 10$ GeV γ-sphere. For a source with flux density in Jy of S_{Jy} an angular diameter distance of D Gpc and observed brightness temperature $10^{12} T_{12}$ K, the radius of the radio photosphere is $r_{rph} \sim 0.1\ \lambda_{mm} D\theta_{-1}^{-1} T_{12}^{-1/2} S_{Jy}^{1/2}$ pc. (Note that the radius of the radio photosphere diminishes with increasing photon energy in contrast to the radius of the γ-sphere.) The measured brightness radio temperatures are $T_{12} \lesssim 1$ (Linfield et al. 1990). Typically for 3C 279 $r_{rph}(1\text{ mm}) \sim 0.1$ pc. For this reason, it is more likely that correlated variability be observed between the flux at wavelengths $\lesssim 1$ mm and energies ~ 10 GeV.

There are two further points of contact between the radio and the γ-ray observations. Firstly VLBI polarization observations indicated surprisingly large degrees of linear polarization with little evidence for Faraday rotation (e.g., Cawthorne et al. 1993). This appears to be true for both the self-absorbed cores and the supposedly optically thin observed jets. So the core emission is essentially produced within one synchrotron absorption length at the radius where the jet becomes optically thick at the observing frequency. We can now compute the average Faraday rotation expected across this absorption length. For simplicity, we suppose that there is a power-law distribution of relativistic electrons in the jet comoving frame $dN_\gamma/d\gamma \propto \gamma^{-p}; \gamma > \gamma_{min}$. The expected rotation will exceed 1 rad and there will be strong depolarization when the observed brightness temperature satisfies

$$T \gtrsim \left(\frac{\Gamma m_e c^2}{3k}\right) \gamma_{min}^{-1/s} (\ln \gamma_{min})^{-1/s} \tag{5.4}$$

(e.g., Jones 1988). For an electron-ion jet with $p \sim 2$, $\Gamma \sim 10$, the fact that strong linear polarization is observed implies that $\gamma_{min} \gtrsim 5 T_{12}^{1/2}$. It seems unlikely that an accumulation of mildly relativistic electrons could be avoided in a jet that expands over several decades of radius. However, if there is an equal number of positrons present, the Faraday rotation vanishes and the linear polarization can reflect the order in the magnetic field.

For this reason, we argue that the radio polarization observations support the pair cascade model and not the relativistic ion model. Similar remarks can be made concerning circular polarization observations. Secondly, modeling the variability of radio jets, especially the intraday variety, leads to the conclusion that radio jets are both radiatively inefficient and particle-dominated, as independently inferred above.

5.5. *γ-Ray Variability*

We have proposed that the γ-ray source, like the radio source, is inhomogeneous. This may be reflected in the energy dependence of the variability. There are two natural possibilities. If we suppose that jets are locally and independently variable at all radii, and that Γ is roughly constant, then we expect that the variations at large radius and high energy should be slower than those observed at small radius and low energy. Alternatively, if the observed variation is attributable to a disturbance like an internal shock that propagates over several octaves of energy, then we also expect the high-energy emission to lag the low-energy emission. To date, only one source, 3C 279, has shown a luminous flare to make a search for these effects practical, and they do not appear to be present in the data (R. C. Hartmann 1994, private communication). It is hoped that enough strong flares will be observed by EGRET to test this prediction more thoroughly. For Mrk 421 at TeV energy the γ-spheric radius is expected to be comparable with that for 3C 279 at GeV energy (cf. eq. [3.21]), suggesting that the variability timescale for Mrk 421 at TeV should be comparable with that for 3C 279 at 1 GeV, ~ 2 days. Naturally, any convincing correlation of γ-ray variations with changes in other regions of the electromagnetic spectrum would be highly diagnostic of the relative locations of emission.

5.6. *The Inner Jet*

In §§ 5.1 and 5.4, we have tentatively argued that γ-ray jets are carried along by the momentum residing in their low-energy pairs (as opposed to electromagnetic field or relativistic protons) at least beyond their annihilation radii. This has not explained how they are collimated and accelerated to ultrarelativistic speed. For the best-studied case of 3C 279 the location of the annihilation threshold depends upon the unknown intensity of the Thomson-scattered radiation at an energy ~ 100 keV. However, this is likely to be larger than the putative size of the black hole, and a means of transporting energy and momentum out to this radius must be postulated if the black hole is identified as the primary energy source. We call the zone $r \lesssim r_{ann}$, the *inner jet*.

Can this energy and momentum be carried by subrelativistic pairs? Here there is a constraint because all pairs can cool to subrelativistic energy on a dynamical timescale, and two-photon, electron-positron annihilation, demonstrably unimportant at larger radii, becomes significant and limits the pair density within the jet. (It might be difficult to observe the 0.5 MeV annihilation line as it will carry only a small fraction of the total γ-ray power. In any case, it is expected to be broadened and blueshifted.)

Specifically, if we equate the pair annihilation time in the comoving frame to the dynamical timescale, then we find that the maximum thrust that can be associated with a jet at a radius $r \lesssim r_{\rm ann}$ is given by

$$P_{\pm} \lesssim 10^{35}\left(\frac{e}{10^{15}\ \rm cm}\right)\left(\frac{\Gamma}{10}\right)^3\left(\frac{\theta}{0.1}\right)^2\ \rm dyne\ . \tag{5.5}$$

At small radii, this is smaller than the inferred thrusts of both the γ-ray and radio jets. We conclude that some alternative carrier of energy and momentum must be present for $r \ll r_{\rm ann}$ if it is generally true that the high-energy γ-ray spectrum continues down to energies of order a few MeV solely in the CRS. This point has also been made independently by Ghisellini & Maraschi (1989).

There are two natural alternatives for transporting energy and momentum from the vicinity of the black hole to the annihilation threshold. First, if a beam of ultrarelativistic ions can be accelerated with Lorentz factors $\Gamma \sim 10$, then these can carry ample energy, ~ 5 GeV for each electron, to account for the particle acceleration of relativistic electrons in the γ-ray jet. Alternatively, as has been reviewed elsewhere (e.g., Blandford 1989), the initial energy extraction and transport may be electromagnetic in character.

5.7. *The Disk, Black Hole Connection, and the FR1/FR2 Dichotomy*

One possible mechanism for creating electromagnetic jets postulates that a large-scale poloidal magnetic field thread the accretion disk and the black hole (see Fig. 6). The disk, being a good conductor, will convect and wind up the magnetic flux, driving a hydromagnetic wind in which a centrifugally driven outflow is collimated by both the hoop stress of the toroidal magnetic field and magnetic pressure gradients. The characteristic outflow speed from a particular disk radius is estimated to be several times the Keplerian speed. The poloidal jet velocity should therefore diminish roughly as the inverse square root of the cylindrical radius.

If magnetic flux also penetrates the event horizon of the black hole, then the spin energy of the hole can also be extracted with an estimated efficiency of $\sim 50\%$. This, it is proposed, sustains the relativistic jet core (e.g., Thorne, Price, & MacDonald 1986).

This model provides a qualitative explanation for the difference between FR1 and FR2 sources described in § 2. In sources with either slowly spinning or weakly magnetized black holes, the relativistic core will be weak as will also be the resulting jet. As the jet flow develops, magnetic stresses will decelerate the core transferring its linear momentum radially outward, and producing a slow combined jet moving with the speed characteristic of the outflow at large radius: an FR1 source. Conversely, when a powerful, relativistic core is produced, the slow-moving sheath will be accelerated up to mildly relativistic speed: an FR2 source.

5.8. *Radio-loud and Radio-quiet AGNs*

We conclude by addressing the most fundamental division in the taxonomy of AGNs that between the minority of radio-loud sources and the majority of radio-quiet sources. Any physical explanation of this difference must account for the durability of the radio loudness as implied by the absence of coreless extended radio sources. One important clue is that the radio-quiet Seyfert galaxies are associated with spiral galaxies, whereas radio galaxies are associated with ellipticals. It is not known whether or not this pattern extends to the quasars, but we suppose that this is the case.

The *CGRO* results have added a further clue. The EGRET sources are associated with compact radio sources. By contrast, OSSE and COMPTEL observations of the nearby radio-quiet AGNs (Cameron et al. 1993) have shown that they only emit γ-rays of energy $\lesssim 50$ keV, apparently isotropically and presumably from quite close to the central black hole. This supports the natural inference that was drawn pre-*CGRO*, that it is the formation and collimation of a relativistic jet that is the key characteristic of a radio-loud nucleus.

A promising explanation for the difference between the two classes of AGNs is that although the accreting gas always forms a magnetized disk, in the case of spiral galaxies there are sufficient mass-losing stars at high latitude to prevent a hydromagnetic wind from becoming super-Alfvénic and self-collimating (e.g., Blandford 1989). There may still be a central spinning black hole from

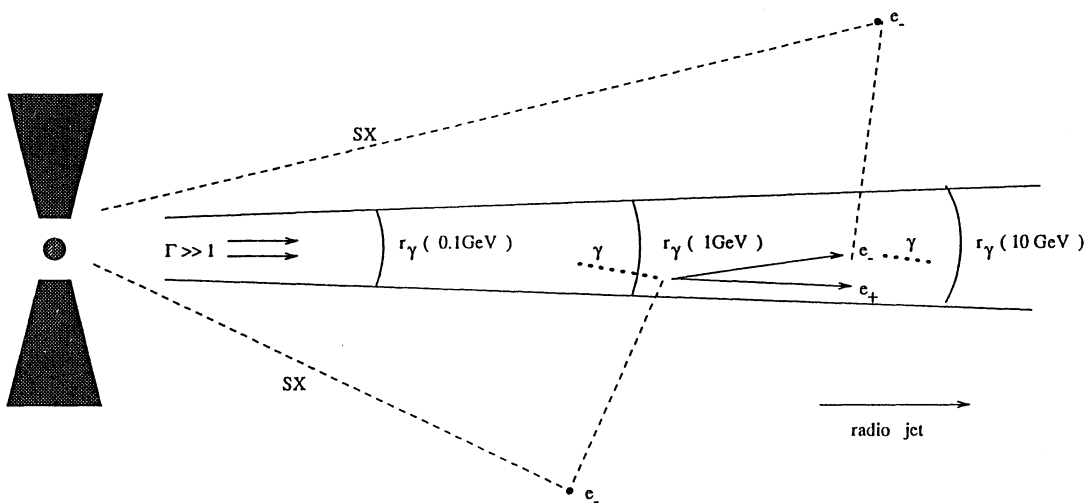

FIG. 6.—Schematic representation of the pair cascade model. A relativistic jet is formed parallel to the spin of a massive black hole orbited by a thick accretion disk. Soft X-ray photons denoted SX emitted near the black hole may be Thomson-scattered into the jet. There they can both combine with γ-rays to form electrons and positrons and be inverse Compton scattered by electrons and positrons to form γ-rays. In this way a pair cascade can develop. Also shown are the γ-spheres for $E_\gamma = 0.1, 1, 10$ GeV.

which energy is extracted electromagnetically and outflow. However, in the absence of a collimating toroidal field, the outflow will be quasi-spherical, and so a tightly collimated, relativistic jet will not form. This quasi-spherical wind may be radiatively accelerated and may also account for the broad absorption lines that are believed to be characteristic of radio-quiet quasars (e.g., Turnshek 1988). By contrast, we posit that the nuclei of elliptical galaxies contain a much older and more tenuous stellar population that do not inject enough mass into the outflow to change its angular momentum appreciably. Here, a self-collimated MHD wind may arise more naturally, although it may also be necessary to extract energy and angular momentum from several decades of disk radius. It is hoped that by probing relativistic jets on smaller scales than those accessible to radio astronomy, high-energy γ-ray observations will test this and alternative explanations for their origin.

We thank M. Begelman, P. Coppi, M. Rees, Y. C. Lin, P. Michelson, P. Nolan, A. Laor, and especially M. Sikora for useful discussions. We also thank the referee for stimulating us to clarify the text in several places. This work was supported by NASA grants NAGW 2816, 2372, and NAG 2504.

APPENDIX

EMISSION IN THE AGN FRAME

In § 4 we computed the inverse Compton γ-ray emission by transforming into a frame moving radially outward along the jet with a Lorentz factor Γ, in which the relativistic electrons and positrons were supposed to have an isotropic distribution function. For simplicity, we supposed that all the material at a given radius moved with this single speed and, furthermore, that there was neither acceleration nor deceleration along the jet. As these assumptions are highly questionable and as the effects of Doppler beaming are large, this might be thought to diminish the value of the models. However, this sensitivity to the assumed jet kinematics is, in one sense, illusory, and it is the purpose of this appendix to demonstrate this.

An alternative and equivalent approach to that presented in § 4 is to continue to work exclusively in the AGN frame. The pair distribution function must then be defined in terms of the total particle energy in this frame. The pair distribution function must then be defined in terms of the total particle energy in this frame. Furthermore, provided that the opening angle of the jet is small, we can treat this distribution function as one-dimensional. This allows us to compute theoretically the total power *radiated* by the jet as γ-rays and *carried* in the form of pairs. This is the quantity that is of most immediate interest because it is the inferred γ-ray powers that provide the greatest challenge to our understanding of jets as derived from radio astronomy. (As we are ignorant of the beam pattern of jets, it is not, in general, possible to compute the distribution with observer orientation of the *flux* unless we make simplistic assumptions like assuming that the bulk Lorentz factor is constant both across and along the jet.)

If we work with an AGN-based energy distribution function, then individual particles will not conserve their energy on the gyrational timescale, and will spend a small fraction of their orbits actually moving radially inward. In the AGN-based approach, we simply ignore those electrons and positrons that, at a given instant, are not outwardly directed, and (provided that $\Gamma \gg 1$) this only introduces errors $O(\Gamma^{-2})$ in the computed power. In this approach, the comoving frame particle acceleration is combined with the expansion losses as described in § 4 plus any changes in the bulk velocity of the flow by specifying an essentially ad hoc average source function (*in the AGN frame*). As we have no basis for specifying this source function in either frame, neither approach is to be preferred. If the injection is predominately at energies well in excess of the EGRET range, or in the form of a flat power law, it can be shown that the two approaches are effectively equivalent.

Working, therefore, in the AGN frame, pair production is handled using equation (4.9) and (4.11), adjusted so that the primed quantities evaluated in the comoving frame are now replaced by unprimed quantities evaluated directly in the AGN frame. The pair production function is given by

$$\tilde{\eta}_{pe} = 2\pi \int_{-1}^{1-2/E_\gamma} d\mu (1-\mu) \int_{\ln[E_\gamma/2(1-\mu)E_e(E_\gamma - E_e)]} d\ln E_s \tilde{I}_s \frac{d\sigma_p}{d\ln E_e} .$$

The dimensionless pair production opacity is given by equation (3.1)

To treat the Compton scattering, we consider an ultrarelativistic electron or positron with initial energy E_{ei} measured in the AGN frame that scatters a soft photon and recoils with energy E_{ef} significantly smaller than E_{ei}. We ignore the energy of the soft photon so that the final γ-ray energy is $E_\gamma = E_{ei} - E_{ef}$. If we again introduce direction cosines μ, μ^{ER} in the AGN and electron rest frames with respect to the initial electron (or positron) momentum, we obtain

$$E_\gamma = \frac{E_{ei}^2 E_s (1-\beta_{ei}\mu)(1-\mu^{ER})}{1 + E_{ei} E_s (1-\beta_{ei}\mu)(1-\mu^{ER})} , \tag{A1}$$

where $\beta_{ei} = (1 - E_{ei}^{-2})^{1/2}$.

The Klein-Nishina cross section (in units of the Thomson cross section) can be written in the form

$$\frac{d\sigma_{KN}}{d\ln E_{ef}} = \frac{1}{(1-r)} \frac{d\sigma_{KN}}{d\ln E_\gamma} = \frac{3}{8} \frac{[r + r^{-1} - 1 + (\mu^{ER})^2]}{E_s E_{ei}(1-\beta_{ei}\mu) r} , \tag{A2}$$

where

$$r = \frac{E_s^{ER}}{E_\gamma^{ER}} \simeq 1 + E_{ei} E_s (1-\beta_{ei}\mu)(1-\mu^{ER}) = \frac{E_{ei}}{E_{ef}} \tag{A3}$$

is the ratio of the initial to the final photon energy in the electron rest frame under our approximation. The Compton redistribution functions are then given by

$$\tilde{\eta}_{ce}(E_{ei}, E_{ef}) = 2\pi \int_{-1}^{1} d\mu(1 - \beta_{ei}\mu) \int_{\ln[(E_{ei}-E_{ef})/2E_{ei}E_{ef}(1-\beta_{ei}\mu)]} d\ln E_s \tilde{I}_s(r\mu, E_s) \frac{d\sigma_c}{d\ln E_{ef}} \tilde{\eta}_{c\gamma}(E_{ei}, E_\gamma)$$

$$= 2\pi \int_{-1}^{1} d\mu(1 - \beta_{ei}\mu) \int_{\ln[(E_{ei}-E_{ef})/2E_{ei}E_{ef}(1-\beta_{ei}\mu)]} d\ln E_s \tilde{I}_s(r, \mu, E_s) \frac{d\sigma_c}{d\ln E_\gamma} . \quad \text{(A4)}$$

The dimensionless Compton scattering opacity is given by

$$\tilde{\kappa}_c = 2\pi \int_{-1}^{1} d\mu(1 - \beta_{ei}\mu) \int d\ln E_s \tilde{I}_s \left(\frac{d\sigma_c}{d\ln E_\gamma} \right) .$$

The coupled equations for the number densities of γ-rays and pairs per unit jet length and per unit log $E_{\gamma,e}$ measured in the AGN frame, and equivalent to equations (4.5) and (4.6), are now

$$\frac{\partial N_\gamma}{\partial \ln r} = -\tilde{\kappa}_p N_\gamma + \int_{\ln E_\gamma} d\ln E_{ei} \tilde{\eta}_{c\gamma}(E_{ei}, E_\gamma, r) N_e(E_{ei}, r)$$

$$\frac{\partial N_e}{\partial \ln r} = -\tilde{\kappa}_c N_e \int_{\ln E_e} d\ln E_{ei} \tilde{\eta}_{ce}(E_{ei}, E_e, r) N_e(E_{ei}, r)$$

$$+ \int_{\ln E_e} d\ln E_\gamma \tilde{\eta}_p(E_\gamma, E_e, r) N_\gamma(E_\gamma, r) + S(E_e, r) , \quad \text{(A5)}$$

where $\tilde{S}$ is the AGN frame source function.

Equation (A5) have also been integrated using similar sets of parameters to those adopted in § 4. As expected, the results are quite similar, showing that the spectral power of the γ-rays is insensitive to the detailed kinematic assumptions.

REFERENCES

Antonucci, R. 1993, ARA&A, 31, 473
Barthel, P. 1993, Nature, 362, 326
Begelman, M. C., & Sikora, M. 1987, ApJ, 322, 650
Blandford, R. D. 1989, in Theory of Accretion Disks, ed. P. Meyer, W. Duschl, J. Frank, & E. Meyer-Hofmeister, 35
———. 1993, in Compton Gamma Ray Observtory, ed. N. Gehrels & M. Friedlander (New York: American Institute of Physics), 533
Blandford, R. D., & Rees, M. J. 1974, MNRAS, 169, 395
Bloom, S. D., & Marscher, A. P. 1993, in Compton Gamma Ray Observatory, ed. N. Gehrels & M. Friedlander (New York: American Institute of Physics), 578
Bridle, A. H., & Perley, R. A. 1984, ARA&A, 22, 319
Cameron, R. A., et al. 1993, in Compton Gamma Ray Observatory, ed. N. Gehrels & M. Friedlander (New York: AIP), 478
Cawthorne, T. V., et al. 1993, ApJ, 416, 496
Coppi, P., & Blandford, R. D. 1990, MNRAS, 245, 453
Coppi, P., Kartje, F. J., & Königl, A. 1993, in Compton Gamma Ray Observatory, ed. N. Gehrels & M. Friedlander (New York: American Institute of Physics), 559
Dermer, C., & Schlickheiser, R. 1993, ApJ, 416, 458
———. 1993, ApJS, 90, 945
Dermer, C., Schlickheiser, R., & Mastichiadis, A. 1992, A&A, 256, L27
Fichtel, C. E., & Thompson, D. J. 1994, in High Energy Astrophysics, ed. J. Matthews, in press
Fichtel, C. E., et al. 1994, ApJS, 94, 551
George, I. M., Warwick, R. S., & Bromage, G. E. 1988, MNRAS, 232, 793
Ghisellini, G., & Maraschi, L. 1989, ApJ, 340, 181
Gould, R. J., & Schréder, G. P. 1967, Phys. Rev., 155, 1404
Hartman, R. C., et al. 1992, ApJ, 385, L1
Hermsen, W., et al. 1993, A&A, 97, 97
Hoshino, M., et al. 1992, ApJ, 390, 454
Jones, F. C., & Ellison, D. 1991, Space Sci. Rev., 58, 259
Jones, T. W. 1988, ApJ, 332, 678
Kniffen, D. A., et al. 1993, ApJ, 411, 133
Königl, A. 1981, ApJ, 243, 700
Kormendy, J. 1992, in Testing the AGN Paradigm ed. S. Holt, S. G. Neff, & C. M. Urry (New York: American Institute of Physics), 23
Laing, R. A. 1992, in Astrophysical Jets, ed. D. Burgarella, M. Livio, & C. O'Dea (Cambridge: Cambridge Univ. Press), 95
Laor, A. 1990, MNRAS, 246, 369
Laor, A., et al. 1994, ApJ, 435, 611
Lawrence, A., & Elvis, M. 1982, ApJ, 256, 410
Lin, Y. C., et al. 1993, ApJ, 416, L53
Linfield, R. P., et al. 1990, ApJ, 385, 350
Makino, F., et al. 1989, ApJ, 347, L9
Mannheim, K. 1992, A&A, 269, 67
Maraschi, L., Ghisellini, G., & Celotti, A. 1992, ApJ, 397, L5
Marscher, A. P., & Gear, W. K. 1985, ApJ, 298, 114
McHardy, M., et al. 1994, in IAU Symp. 159, Active Galactic Nuclei across the Electromagnetic Spectrum (Dordrecht: Reidel), 153
Melia, F., & Königl, A. 1989, ApJ, 340, 162
Netzer, H. 1992, in Active Galactic Nuclei, ed. R. D. Blandford, H. Netzer, & L. Woltjer (Berlin: Springer), 57
Pearson, T. 1989, in Parsec Scale Radio Jets, ed. A. Zensus & T. Pearson (Cambridge: Cambridge Univ. Press), 1
Punch, M., et al. 1992, Nature, 358, 477
Quirrenbach, A., et al. 1991, ApJ, 372, L71
Rees, M. 1967, MNRAS, 137, 429
Shields, G. A., & McKee, C. F. 1981, ApJ, 246, L51
Sikora, M., Begelman, M., & Rees, M. 1994, ApJ, 421, 153
Thompson, D. J., Bertsch, D. L., Dingus, B. L., Fichtel, C. E., & Hartman, R. C. 1993, ApJ, 415, L13
Thorne, K. S., Price, R. M., & MacDonald, D. A. 1986, Black Holes: The Membrane Paradigm (New Haven: Yale Univ. Press)
Turnshek, D. 1988, QSO Absorption Lines, ed. C. Blades, D. Turnshek, & C. Norman (Cambridge: Cambridge Univ. Press), 17
Wilkes, B. J., & Elvis, M. 1987, ApJ, 323, 243